diversity

MDPI

Article

New Species of *Vegavis* (Neornithes) from Antarctica Highlights Unexpected Cretaceous Antarctic Diversity

Facundo Irazoqui [1,2,*], Carolina Acosta Hospitaleche [1,2,*], Ariana Paulina-Carabajal [2,3,4], Paula Bona [2,5] and Nahuel Vega [6]

1 Vertebrate Paleontology Division, La Plata Museum, Faculty of Natural Sciences and Museum, National University of La Plata, La Plata B1900FWA, Argentina
2 National Council for Scientific and Technical Research (CONICET), Godoy Cruz 2290, Ciudad Autónoma de Buenos Aires C1425FQB, Argentina
3 Institute for Research on Biodiversity and the Environment (INIBIOMA)-CCT Patagonia Norte, Av. de los Pioneros 2350, San Carlos de Bariloche R8400, Argentina
4 Museo de la Asociación Paleontológica Bariloche, Av. 12 de Octubre y Sarmiento, San Carlos de Bariloche R8400, Argentina
5 Vertebrate Paleontology Division, La Plata Museum Annex II, Faculty of Natural Sciences and Museum, National University of La Plata, 122nd and 60th streets, La Plata B1900, Argentina
6 Argentine Neutron Beam Laboratory, National Atomic Energy Commission Av. General Paz 1499, Villa Maipú B1650, Argentina; nahuelvega@cnea.gob.ar
* Correspondence: facundopaleo@gmail.com (F.I.); acostacaro@fcnym.unlp.edu.ar (C.A.H.)

Abstract

A fossil bird (MLP-PV 15-I-7-52) from Marambio (Seymour) Island, Antarctica, is described, representing the best-preserved skull reported for a Cretaceous neornithine and associated postcranial elements. Morphological analysis of the articular portion of the mandible, the pterygoid, and the femur supports the assignment of this specimen to the genus *Vegavis*. The palatine morphology exhibits a combination of plesiomorphic and autapomorphic characters within Neognathae. Substantial differences in the size relationship between the ala preacetabularis and the femur, as well as differences between the femora of *V. iaai* and MLP-PV 15-I-7-52, indicate that the latter represents a new species of *Vegavis*. In addition, a third species of *Vegavis* is proposed based on the AMNH FARB 30899 specimen, previously assigned to *V. iaai*, which exhibits substantial differences with the above-mentioned specimens, particularly in the mandibular morphology.

Keywords: Aves; Galloanseres; Aequornithes; Marambio (Seymour) Island; López de Bertodano Formation; skull anatomy

Academic Editor: Michael Wink

Received: 22 December 2025
Revised: 24 January 2026
Accepted: 28 January 2026
Published: 30 January 2026

1. Introduction

Vegavis iaai is a Mesozoic neornithine bird from Vega Island, Antarctica, known from at least three specimens, which provide robust fossil evidence for the emergence of Neornithes in the Late Cretaceous [1,2]. Two specimens (MLP-PV 93-I-3-1 and MACN-Pv 19.748) were found in concretions within sediments of the Sandwich Bluff Member of the López de Bertodano Formation. The holotype of *V. iaai*, MLP-PV 93-I-3-1, consists exclusively of postcranial remains, including the pelvis, synsacrum, femur, tibiotarsus, and tarsometatarsus. It was first described by Noriega and Tambussi (1995) [3] prior to the proposal of the species, and later by Clarke et al. (2005) [1] when the new taxon was formally erected. Subsequently, Acosta Hospitaleche and Worthy (2021) [4] provided new

descriptions of these elements after extracting them from the sedimentary matrix, revealing novel anatomical information about this taxon.

The second specimen, MACN-Pv 19.748 (in addition to contributing significant postcranial remains that showed slight size variation compared to the holotype), includes part of the vocal organ (syrinx), the articular portion of the mandible, and a pterygoid [2,5]. Recently, a third specimen, AMNH FARB 30899, was reported, consisting of a partial skull including its natural endocast, the basicranium, the anterior portion of the palatines, a partial beak, and an almost complete mandible [6]. Its specific assignment was based on the comparison of the mandibular articular portion with specimen MACN-Pv 19.748 [6–8].

Two other specimens have been referred to *V. iaai* or to *Vegavis* with less certainty: a synsacral fragment comprising three vertebrae (MN 7832-V) assigned to *Vegavis* cf. *V. iaai* [9], and a femur preserved in two fragments, previously considered a cariamiform [10] and later assigned to *Vegavis* sp. [11]. The latter shows notable differences in size from the *V. iaai* holotype.

The phylogenetic relationships of *Vegavis* within Aves remain far from resolved, despite numerous phylogenetic analyses including the two most complete specimens [e.g., [1,2,4–8,12–14]]. The results of these analyses are highly variable, with *Vegavis* being recovered either within or outside Neornithes (e.g., [13]). A brief historical overview of proposed taxonomic placements for *Vegavis* includes the following: as a presbyornithid [3]; as a member of crown-group Anseriformes closely related to (or positioned within) Anseres [1,2,6], as a stem-group member of Anseriformes [12]; and within the new family Vegaviidae alongside other Maastrichtian taxa such as *Neogaeornis wetzeli* from Chile and *Polarornis gregorii* from Marambio Island, along with *Australornis lovei* from the Paleocene of New Zealand [15]. However, even in the absence of an alternative phylogenetic proposal, the erection of Vegaviidae was criticized for lacking verifiable characters shared by all included taxa [16]. Around the same time, the new species *Maaqwi cascadensis* from the Campanian of Hornby Island, Canada, was also included within Vegaviidae [17].

The description and analysis of a new specimen from the López de Bertodano Formation (Marambio Island, Antarctica) brings renewed attention to Cretaceous birds. This partial skeleton (MLP-PV 15-I-7-52) comprises both cranial and postcranial remains, as well as a natural cranial endocast, which allows for its referral to the genus *Vegavis*. In this contribution, we discuss the qualitative and quantitative variations observed among the different specimens assigned to *Vegavis iaai* and propose two new species.

2. Materials and Methods

The specimen MLP-PV 15-I-7-52 and the holotype of *Vegavis iaai* MLP-PV 93-1-3-1 are housed at the Colección Paleontología Vertebrados del Museo de La Plata (MLP-PV), La Plata, Argentina. The new specimen was preserved as associated materials within a single concretion. The skull, mandibles, pelvis and synsacrum, and tarsometatarsus were mechanically removed from the surrounding sedimentary matrix. The quadrate, quadratojugal, pterygoid, palatine, and a posterior cervical vertebra were digitally extracted through segmentation of CT-scan data (Supplementary Material Figure S1).

Anatomical and topographical terms follow Baumel and Witmer (1993) [18] for general osteology and cranial foramina, and Mayr (2016) [19] for the hypotarsus. Some terms, such as “processus coronoideus”, “rostral process” of the pterygoid, and “processus retroarticularis” of the mandible, are enclosed in quotation marks to denote uncertain homologies. Measurements were taken with a Vernier Caliper with a precision of 0.02 mm.

The three-dimensional non-destructive characterization of the sample was performed using high-resolution X-ray computed tomography (micro-CT) with a Nikon Metrology XT H 225 ST 2x system (Nikon Metrology UK Ltd., Castele Donington, Derby, UK). The

instrument was operated with a microfocus X-ray tube using a tungsten target at 95 kV and 211 µA, with a 1 mm aluminium filter, yielding an isotropic voxel size of 31 µm. A total of 2500 projections were acquired over 360° using a standard scanning mode. Reconstruction of the raw data was carried out using Inspect-X XT 6.13 (Nikon Metrology).

Body masses of fossil taxa were calculated using the equations proposed by Field et al. (2013) [20] based on femoral and humeral circumferences and the facies humeralis of the coracoid.

The description of the *Vegavis iaai* specimens includes the catalogue number of each specimen when the skeletal elements are present in all individuals.

3. Geological Setting

Marambio (Seymour) Island (Figure 1A) forms part of the James Ross Island group (Figure 1C,D) at the northeastern tip of the Antarctic Peninsula (63°30′–65° S, 57–58° W). The island preserves the youngest infill of the James Ross Basin, represented by a sedimentary succession (Figure 1B) spanning the Maastrichtian–early Paleocene Marambio Group and the late Paleocene–Oligocene Seymour Island Group [21–24].

The Marambio Group [20] spans the Campanian–Paleocene and comprises the Haslum Crag, López de Bertodano, and Sobral formations [21,24,25]. The López de Bertodano Formation (Figure 1A,B) unconformably overlies the Haslum Crag Formation, separated by an erosional discontinuity [21,25], and is, in turn, unconformably overlain by the Sobral Formation [24]. The succession mainly consists of sandy mudstone, muddy siltstone, and silty very fine sandstone, interbedded with concretionary horizons [22,25]. Fossil content includes marine invertebrates, vertebrate remains, invertebrate trace fossils, and carbonized wood [22,25,26].

The formation is subdivided into cartographic units 2–9 (equivalent to Klb 2–9 of Macellari, 1988 [22]), which exhibit progressive lithological transitions and are differentiated by degree of lithification, sand-to-mud ratios, and fossil abundance [22,25]. These units are grouped into three allomembers. The lower Rotularia Allomember (units 2–6) and the overlying Molluscan Allomember (units 7–9) are Maastrichtian in age, whereas the uppermost Cenozoic Allomember (units 10–11) is assigned to the Danian [22,24,25].

The specimen MLP-PV 15-I-7-52 was recovered from Unit 9 of the Molluscan Allomember (Figure 1B), a level characterized by abundant molluscan fossils [22,27]. This unit crops out in the southern sector of Marambio Island (Figure 1A), within a belt extending between López de Bertodano Bay and the Weddell Sea [22,24]. Unit 9 reaches approximately 180 m in thickness and is dominated by poorly consolidated gray sandy mudstone, intercalated with lithified fine sandstone beds and abundant carbonate concretions [22]. Its upper limit is marked by a laterally extensive glauconitic sandstone bed (subunit 9g), which defines the Cretaceous–Paleogene (K–Pg) boundary in the area [22,25]. This glauconitic horizon can be traced for more than 7 km and constitutes the most extensive and the southernmost K–Pg boundary worldwide [25,28].

Immediately below the glauconitic K–Pg marker lies a 20–30 m thick interval of massive gray mudstone with thin sandstone lenses and small concretions [24], several of which preserve exceptional avian remains [14], including the specimen described here.

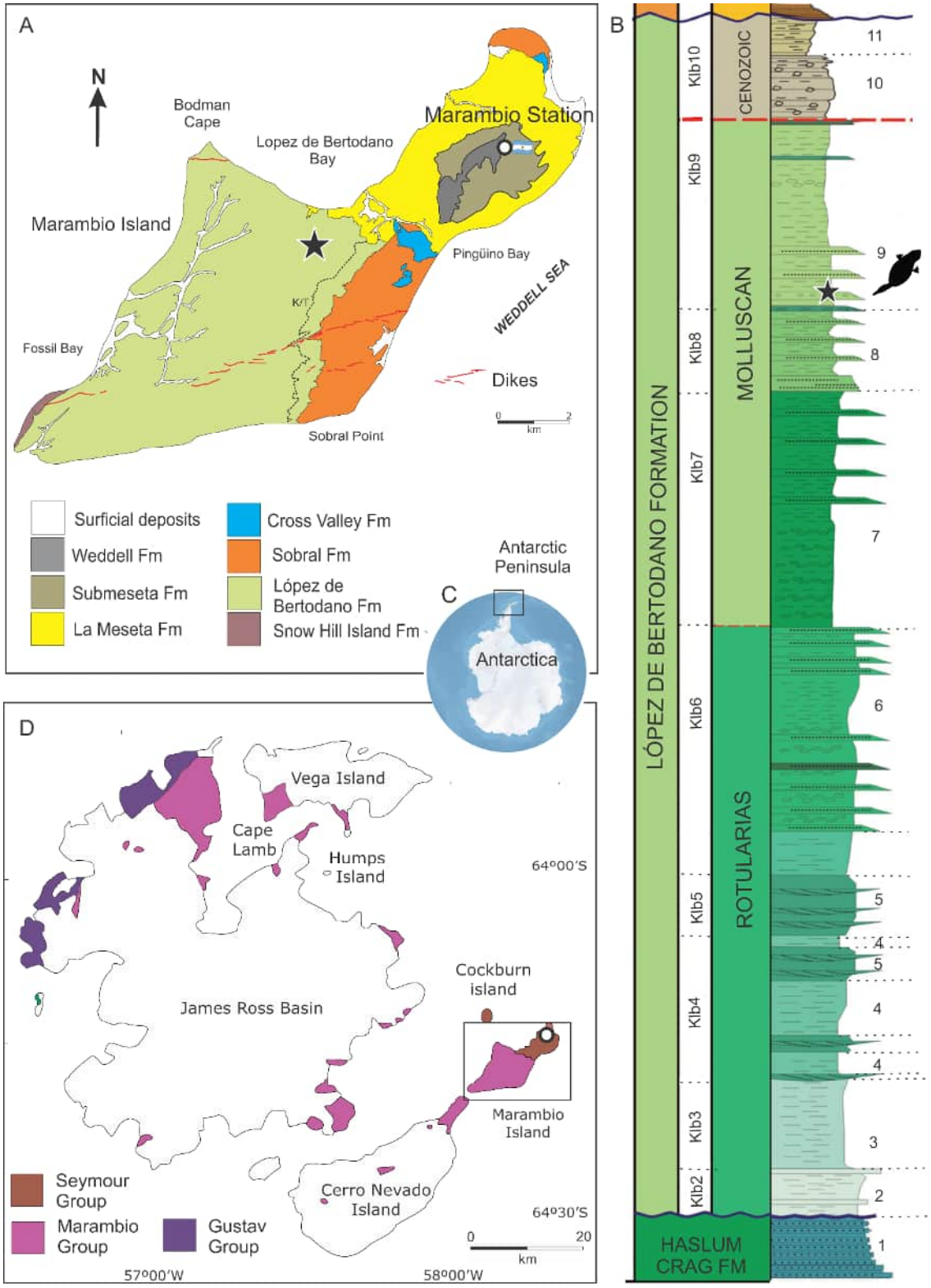

Figure 1. Fossiliferous locality where *V. geitononesos* was collected. (**A**) Marambio Island, (**B**) stratigraphic column, (**C**) Antarctic Peninsula, and (**D**) James Ross Basin. Modified from Montes et al. (2019) [24].

4. Systematic Paleontology

Aves Linnaeus, 1758.

Neornithes Gadow, 1893.

MLP-PV 15-I-7-52 is assigned to crown-group birds based on the following characters, listed in Torres et al. (2025) [6]:

1. Loss of teeth (at least in the mandible of MLP-PV 15-I-7-52).
2. A hyperinflated cerebrum with ventrally shifted optic lobes (inferred from the endocranial morphology in MLP-PV 15-I-7-52).
3. Distal extension of the condylus lateralis beyond the condylus medialis on the femur.

Neognathae Pycraft, 1900.

Assignment to Neognathae is supported by the following characters, possible synapomorphies *sensu* Field et al. (2020) [13], and present in the specimen MLP-PV 15-I-7-52:

1. Condylae of the quadrate separated by an incisura intercapitularis.
2. Presence of tuberculum preacetabulare.

Vegavis Clarke et al. 2005.

Type species: *Vegavis iaai.*

Emended Diagnosis

Diagnosis for *Vegavis* is based on Clarke et al. (2005, 2016) [1,2], Acosta Hospitaleche and Worthy (2021) [4], Álvarez Herrera et al. (2024) [5], Torres et al., (2025) [6] and this study. Asterisks (*) indicate characters present in the new specimen MLP-PV 15-I-7-52.

1. Deeply excavated fossa temporalis bounded rostrally by the steep, shelf-like frontoparietal contact and ventrally by a sharp, dorsoventrally compressed ridge. *
2. Pterygoid with three anterior, pointed processes and a fan-shaped facies articularis quadratica forming a double articulation with the quadrate. *
3. Facies articularis quadratica strongly bent laterally. Rostral pterygoid process spiralled and tapered. *
4. Mandible with cotylae lateralis and medialis arranged almost perpendicular to the ramus mandibulae. *
5. Deep mandibular neurovascular canal closer to the dorsal margin than to the ventral, making the ventral portion higher than the dorsal one. *
6. Well-defined tuberculum laterale. *
7. Presence of a fossa at the rostromedial margin of the cotyla lateralis of the mandible [6]. *
8. Crista transversa of the mandible with a concave rostral surface (modified from [6]). *
9. Lateral crest of mandible projected rostrally.
10. Fossa caudalis with a thick and laterally emarginated caudolateral rim (modified [6]). *
11. Cotyla medialis of the mandible extended caudomedially to the cotyla lateralis, such that the cotyla medialis approaches the lateral margin of the mandible. *
12. Medially projected tubercle on the dorsomedial edge of the mandible, caudal to the "processus coronoideus" (in the sense of mandibular apex). *
13. Femur medially curved, with a proximal rounded fossa [1] *
14. Well-marked laterocaudal scar for the musculus gastrocnemialis lateralis. *
15. Low ridge on the medial edge of the proximal tibiotarsus.

4.1. Vegavis geitononesos sp. nov.

lsid:zoobank.org:act:A3A25B73-2C27-4C13-8C24-3EBAF7FC66CC.

4.1.1. Holotype

MLP-PV 15-I-7-52. Skull lacking the upper beak, with the left side damaged and the right side complete; consisting of the complete right quadrate and pterygoid, the

caudal end of the right palatine, mandibles without symphysis; posterior (tenth?) cervical vertebra and indeterminate fragmentary vertebrae; ribs; incomplete right pelvis including the preacetabular wing of the ilium, proximal portion of the pubis, and part of the ischium; anterior right portion of the synsacrum; distal end of the femur; and proximal half of the right tarsometatarsus.

4.1.2. Derivation of Name

From the Greek words *geítōn* (neighbour) and *nêsos* (island), in reference to the occurrence of this species on Marambio Island, neighbouring Vega Island, the locality of the type species.

4.1.3. Diagnosis

Vegavis geitononesos sp. nov. (MLP-PV 15-I-7-52) differs from *Vegavis iaai* in the following characters:

1. Ala preacetabularis ilii extremely reduced.
2. Acetabulum proportionally larger relative to the ala preacetabularis ilii.
3. Foramina intervertebralia of synsacrum with figure of eight.
4. Femur with narrow sulcus intercondylaris.
5. Subequal rostral extension of the trochlea fibularis and crista fibularis.
6. Linea intermuscularis lateralis expanded proximodistally and laterally, forming a shelf-like projection (distolateral scar [11]).
7. Fossa for insertion of the flexor perforatus digiti II deep, proximolaterally expanded.
8. Tarsometatarsal shaft rounded.
9. Tarsometatarsus with sulcus extensorius deep and wide.
10. Crista dorsalis medialis of the tarsometatarsus lower and broader than the crista dorsalis lateralis.
11. Hypotarsus with a closed canal for flexor digitorum longus.
12. Narrower cotyla lateralis of the mandible.
13. Lateral crest of the mandible extended to the "processus coronoideus".
14. Stronger crista intecotylaris.
15. Thinner processus lateralis mandibulare.

Vegavis geitononesos sp. nov. (MLP-PV 15-I-7-52) differs from *Vegavis notopothousa* sp. nov. (AMNH FARB 30899) in the following characters:

1. Fossa caudalis of the mandible caudally oriented.
2. "Processus retroarticularis" short and ventrally projected.
3. "Processus retroarticularis" separated from the ramus mandibulae through a longer ventral margin.
4. Lateral crest of the mandible extended to the "processus coronoideus".
5. Higher "processus coronoideus".
6. Concave ventral margin of the articular region.
7. Rostrum mandibulare slightly ventrally curved.

4.1.4. Remarks

Additionally, *V. geitononesos* sp. nov. presents the following characters not observed in any other bird:

1. Quadrangular processus basipterygoideus in ventral view, separated from the rostrum parasphenoidale, with lateral articular facets.
2. Elongated processus orbitalis, tapering distally and directed toward the processus basipterygoideus.

4.1.5. Provenance

Unit 9 (Maastrichtian) of the Molluscan Allomember of the López de Bertodano Formation, Marambio Island, Antarctica.

4.2. Vegavis notopothousa sp. nov.

lsid:zoobank.org:act:4CFB9190-3002-4CEC-A4C2-5B3F4D68143A
Figure 7d,i,k,o in Torres et al. (2025) [6].

4.2.1. Holotype

AMNH FARB 30899. Partial skull that includes its natural endocast, basicranium, the anterior portion of the palatines, a partial beak, and an almost complete mandible.

4.2.2. Derivation of Name

From the Greek words *nótos* (south) and *póthos* (longing or nostalgia), in reference to the sense of longing for Antarctica implied by the southern provenance of the fossil and its deposition in a Northern Hemisphere repository.

4.2.3. Diagnosis

Vegavis notopothousa sp. nov. (AMNH FARB 30899) [6] differs from *V. iaai* in the following characters:

1. Narrows and oval cotyla lateralis of mandible.
2. Deeper and laterally displaced fossa in the cotyla lateralis of the mandible.
3. Lateral crest of mandible extended to the level of the tuberculum mediale, without a deep, longitudinal fossa.
4. Fossa caudalis caudodorsally oriented.
5. Crista intercotylaris stronger.
6. "Processus retroarticularis" separated from the ramus mandibulae through a shorter and deeper concave ventral margin.

Vegavis notopothousa sp. nov. (AMNH FARB 30899) [6] differs from *V. geitononesos* sp. nov. (MLP-PV 15-I-7-52) in the following characteristics:

1. Caudal margin of the sulcus glandulae nasalis with a defined boundary.
2. Basisphenoid with fenestrae.
3. More robust medial tubercle of the mandible.
4. Medial tubercle caudally displaced respect to the "processus coronoideus" (in the sense of mandibular apex).
5. Anterior crest of the cotyla lateralis almost perpendicular to the ramus mandibulae.
6. Lateral crest of the mandible rostrally extended to the level of the tuberculum mediale in dorsal view, and not reaching the "processus coronoideus".
7. Fenestra caudalis mandibulae present.
8. "Processus coronoideus" (in the sense of mandibular apex) rounded and lower.
9. Rostrum mandibulare slightly dorsally curved.
10. Convex ventral margin of the articular region of the mandible.
11. "Processus retroarticularis" separated from the ramus mandibulae through a shorter and deeper concave ventral margin.

4.2.4. Remarks

AMNH FARB 30899 was previously assigned to *Vegavis iaai* based on similarities with the caudal mandible of MACN-PV 19.748 (see Torres et al., 2025 [6]).

4.2.5. Provenance

Sandwich Bluff Member, Unit 1 (Maastrichtian) López de Bertodano Formation, Vega Island, Antarctica (Torres et al., 2025 [6]).

5. Results

5.1. Description of V. geitononesos sp. nov. and Comparisons

5.1.1. Skull

The skull of *V. geitononesos* is generally globose, being higher than wide (Figure 2). Cranial sutures are not visible.

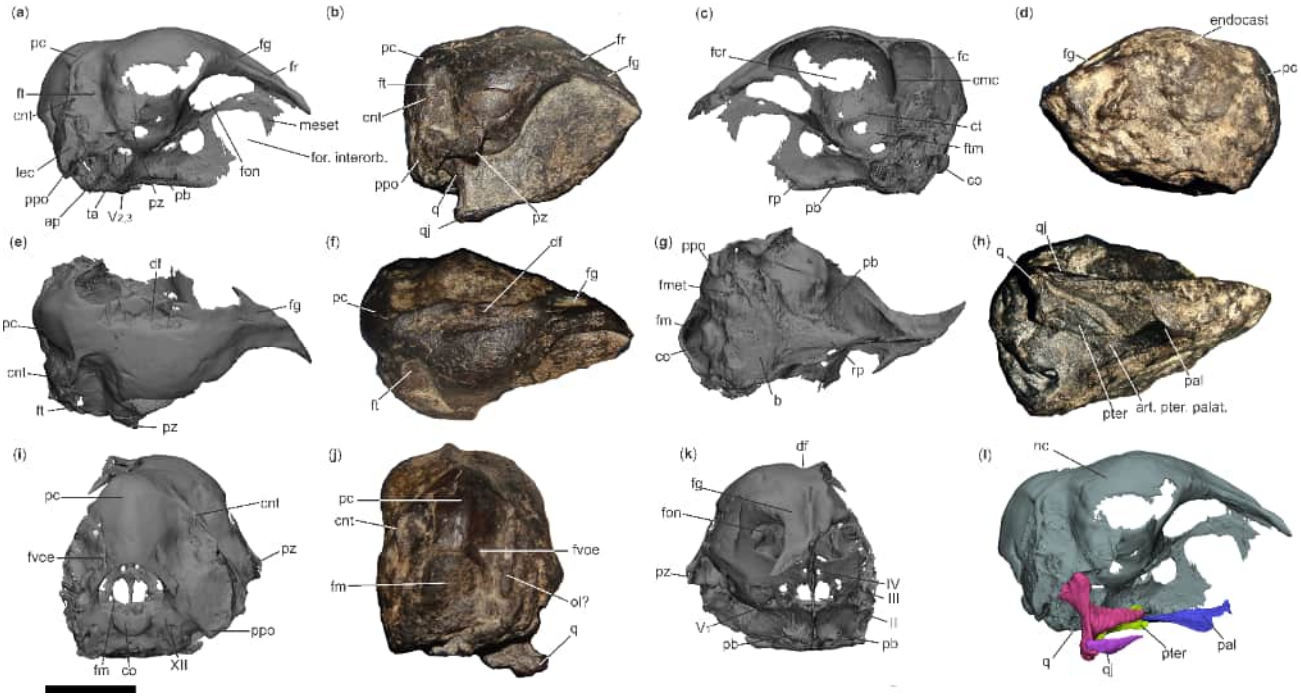

Figure 2. Cranial virtual reconstruction and specimen of *V. geitononesos* sp. nov. (MLP-PV 15-I-7-52). Cranium in (**a**,**b**) right lateral, (**c**,**d**) left lateral, (**e**,**f**) dorsal, (**g**,**h**) ventral, (**i**,**j**) caudal, and (**k**) rostral views. The reconstruction in (**l**) shows the neurocranium-quadrate-quadratojugal-pterygoid-palatine articulations in the right lateral view. Abbreviations: ap, ala parasphenoidalis; art. pter. palat., articulation pterygoid-palatine; b, basisphenoidale; cmc, crista marginalis cerebelli; cnt, crista nuchalis transversa; co, condylus occipitalis; ct, crista tentorialis; df,, depressio frontalis; endocast, natural cranial endocast; fc, fossa cerebelli; fcr, foramen orbitalis cranialis; fg, fossa glandulae nasalis; fm, foramen magnum; fmet, foramen metoticum;; fon, fonticuli orbitocraniales; for. interorb., foramen interorbitalis; fr, frontal; ft, fossa temporalis; ftm, fossa tectum mesencephali; fvoe, foramen venae occipitalis externae; lec, laminae externae cranii; meset, mesethmoidale; nc, neurocranium; ol?, ossified ligament?; pal, palatinum; pb, processus basipterygoideus; pc, prominentia cerebelli; ppo, processus paroccipitalis; pter, pterygoideum; pz, processus zygomaticus; q, quadratum; qj, quadratojugalis; rp, rostrum parasphenoidale; ta, tuba auditiva; V_1, foramen nervi V_1; $V_{2,3}$, foramen nervi $V_{2,3}$; II, foramen nervi II; III, foramen nervi III; IV, foramen nervi IV; XII, foramen nervi XII. Scale bar: 10 mm.

The calvaria is slightly domed, with a deep depression at the caudomedial end of the parietals on both sides of the sagittal midline (Figure 2e,f). However, it is unclear whether this is a taphonomic artifact. The frontals are extremely narrow at the interorbital region (Figure 2e–g), as in *V. notopothousa* (AMNH FARB 30899). However, they form a small midline crest in *V. geitononesos* (Figure 2e), a feature that is not preserved in *V. notopothousa* AMNH FARB 30899. The sulcus glandulae nasale extends caudally over the

dorsal margin of the orbit, with moderate lateral development and without reaching the processus postorbitalis; its caudal margin is only weakly defined (Figure 2f). In contrast, in *V. notopothousa* AMNH FARB 30899, this sulcus extends caudally and lateroventrally to the processus orbitalis, being caudally delimited by a crest [6].

The processus zygomaticus is moderately developed and projects anterolaterally, covering the deep recessus tympanicus dorsalis (Figure 2a,b). The fossa temporalis is deep and extends anteroposteriorly, similar to that of *V. notopothousa* (AMNH FARB 30899) [6], but less than in *Pujatopouli* [14]. No crista temporalis is observed along the anterior margin, which contrasts with the strongly developed crest of *V. notopothousa* (AMNH FARB 30899). *Pujatopouli* exhibits an intermediate condition, with a low but well-defined crest (Torres et al. 2025, extended data Figure 2d) [6]. Posteriorly, the fossa temporalis (Figure 2a,e) is bounded by a broad crista nuchalis transversa that extends laterally forming wing-like projections (Figure 2i). They are less pronounced than in *Pujatopouli*. Laterally, the crista nuchalis transversa bifurcates to form a triangular surface —the lamina externa cranii— which is bounded anteriorly by the crista musculi depressor mandibulare and posteriorly by the crista nuchalis lateralis, as in *Pujatopouli* (Figure 2a); this is not preserved in *V. notopothousa* (AMNH FARB 30899). The crista nuchalis sagittalis is absent, leaving the prominentia cerebellaris smooth along the midline (Figure 2i), in contrast to the short, weakly developed crest in *Pujatopouli*. The prominentia cerebellaris is large and ovoid, as in *Pujatopouli*, but it differs in the dorsal projection, not surpassing the calvaria (Figure 2a,c,i). The processus paroccipitalis projects ventrally to the heart-shaped condylus occipitalis (Figure 2i), as in *Pujatopouli*. Whereas, in *V. notopothousa* AMNH FARB 30899, the processus paroccipitalis projects laterally and does not surpass the condylus occipitalis. The fossa subcondylaris is deep (Figure 2g).

The ala parasphenoidalis is laterodorsally concave anteriorly, enclosing the recessus tympanicus rostralis, as in *Pujatopouli*. The tuba auditiva is completely ossified (Figure 2a,g) and opens in the midline in a dorsoventrally flattened tuba auditiva communis. The processus medialis parasphenoidalis is weakly developed ventrally and acquires a slightly triangular shape, as in *Pujatopouli*. The processus basipterygoideus (Figure 2c,g,k) is dorsoventrally compressed, like in *Cerebavis* [29], but is larger and anteroposteriorly elongated, located halfway along the length of the rostrum parasphenoidale. It appears quadrangular in ventral view, forming a shelf-like platform. The articular surface faces laterally, with a slight ventral tilt, unlike in *Anas*, *Anser*, *Anseranas*, and *Chauna*, where it is predominantly ventral.

In anterior view, large fonticuli orbitocraniales are visible (Figure 2k). Ventromedially to them, two small foramina—corresponding to the nervus trochlearis (CN IV)—face anteriorly (Figure 2k). The internal openings for this nerve are near the midline, above the large circular recess occupied by the optic chiasm. Further ventromedially, two large foramina nervi optici (CN II) open, enclosed by the orbitosphenoids (Figure 2k). These foramina are oval and separate from each other by the mesethmoid, which forms a septum interorbitale that bears a broad fonticulus interorbitali. Endocranially, the optic nerve foramina communicate with a large oval depression that represents the osteological correlate of the optic chiasm. The foramen nervi oculomotori (CN III) is better preserved on the left side, posterior to the foramen of CN IV and dorsal to that of CN II (Figure 2k). The nervi ophthalmici (CN V_1, ophthalmic division of the nervus trigeminus) exits the endocranial cavity through a relatively small foramen, whose external opening faces anteriorly (Figure 2k). This foramen is posterior to the foramen of CN III and opens anteriorly on the laterosphenoid, as in *Pujatopouli*. The larger foramen nervi maxillomandibularis (CN $V_{2,3}$, maxillary and mandibular divisions of the trigeminal nerve) is dorsal and anterior to the ala parasphenoidalis (Figure 2). It is a circular foramen, largely separated anteroposteriorly

from the foramen of CN V_1. The small foramen for the nervus abducens (CN VI) is only observed on the left side. It is located anteroventrally to the foramen of CN V_1 and also faces anteriorly, which is why it is not observed in lateral view of the braincase. There are three small foramina nervi hypoglossi (CN XII) on each side of the wide foramen magnum (Figure 2i). Slightly anteroventrally to them, open two foramina: the largest circular one corresponds to the metotic foramen (for the nervi glossopharyngei, vagus, and accesorius: CNs IX–XI and internal jugular vein), whereas the smallest foramen corresponds probably to the cerebral branch of the internal carotid artery. Further analysis of the CT scans will help to elucidate this. Dorsal and lateral to the foramen magnum are the sulci and foramina venae occipitalis externae.

An extra element on the dorsocaudal surface of the crista nuchalis transversa is interpreted as an ossified cervical ligament (Figure 2j).

5.1.2. Lacrimal

The right lacrimal (Figure 3) is complete and disarticulated from the frontal, suggesting it was not fused to the latter. It features a processus supraorbitalis that is elongated anteroposteriorly (Figure 3a), with a broad articular facet for the frontal (Figure 3c). The processus orbitalis lacrimalis is long, narrow, and exhibits slight torsion (Figure 3b,d); it widens and flattens before terminating in a pointed tip.

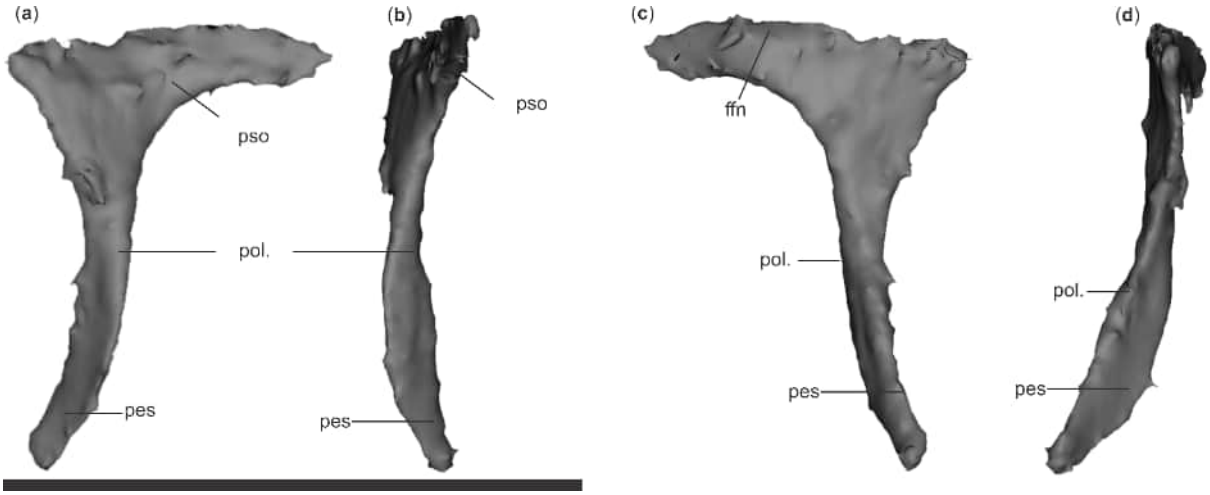

Figure 3. Virtual reconstruction of the right lacrimal of *V. geitononesos* sp. nov. (MLP-PV 15-I-7-52). Lacrimal in (**a**) lateral, (**b**) rostral, (**c**) medial, and (**d**) caudal views. Abbreviations: ffn, facies articularis frontonasalis; pso, processus supraorbitalis lacrimalis; pol., processus orbitalis lacrimalis. Scale bar = 10 mm.

Overall, the lacrimal of *V. geitononesos* is similar to the lacrimal of *V. notopothousa* (Torres et al., 2025: Figure 2) [6]. However, the latter possesses a shorter and less flattened processus orbitalis lacrimalis, and the junction between the processus orbitalis and processus supraorbitalis is broader and more robust.

5.1.3. Quadrate

The right quadrate (Figure 4) is articulated with the skull via the capitulum squamosum and the capitulum oticum, which are separated by a deep incisura intercapitularis (Figure 4b–e). This condition contrasts with that of *Ichthyornis*, in which the incisura intercapitularis is undefined, whereas in *Asteriornis* and *Presbyornis* it is markedly shallow [13,29]. In *Conflicto*, the incisura is poorly developed (contra Tambussi et al., 2019 [30]). The capitulum squamosum projects more dorsally than the capitulum oticum (Figure 4e), whereas

the latter projects more caudally relative to the former. As a result, the capitula does not overlap in lateral views unlike in *Asteriornis*, *Presbyornis* and *Conflicto* [13,30–32].

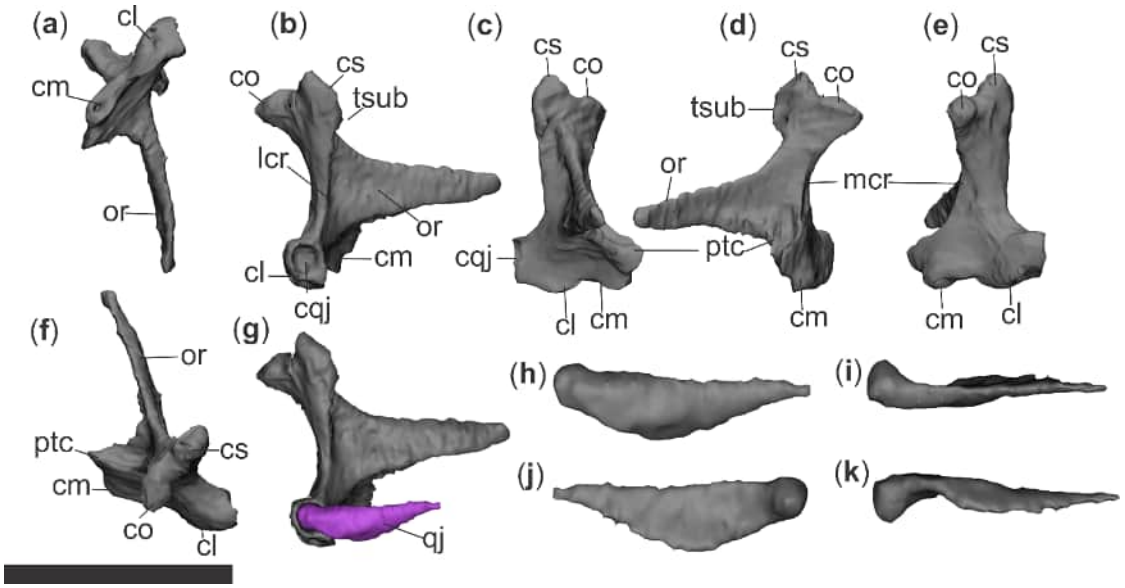

Figure 4. Virtual reconstructions of the right quadrate and quadratojugal of *V. geitononesos* sp. nov. (MLP-Pv 15-I-7-52). Quadrate in (**a**) ventral, (**b**) lateral, (**c**) rostral, (**d**) medial, (**e**) caudal, and (**f**) dorsal views. Right quadrate and quadratojugal in (**g**) lateral view. Quadratojugal in (**h**) lateral, (**i**) dorsal, (**j**) medial, and (**k**) ventral views. Abbreviations: cl, condylus lateralis; cm, condylus medialis; co, condylus oticum; cqj, cotyla quadratojugalis; cs, condylus squamosum; lcr, lateral crest; mcr, medial crest; or, processus orbitalis; ptc, processus pterygoideus; qj, quadratojugal; tsub, tuberculum subcapitulare. Scale bar = 10 mm.

A small tuberculum subcapitulare is attached anteroventrally to the capitulum squamosum, (Figure 4b). It is elongated proximodistally and projects anteriorly. In *Asteriornis*, the tuberculum subcapitulare is lateroventral to the capitulum squamosum, like in *Conflicto*, and is separated from it by a fossa [32] (Figure 7). Ventral to the tuberculum subcapitulare, a well-defined lateral crest (Figure 4b) is distinguished, bounding an anterior fossa at the base of the processus orbitalis.

The lateral and medial condyles are aligned lateromedially (Figure 4c,e). They narrow anteroposteriorly (Figure 4b,d), as in *Asteriornis* and *Presbyornis*, but unlike *Conflicto*, in which the condyles are rounded. However, in *V. geitononesos* the alignment is more precise, whereas in *Ichthyornis*, *Asteriornis*, and *Presbyornis*, the medial condyle is slightly oblique relative to the lateral condyle [32]. The lateral condyle is oval, with its major axis oriented posterolaterally–anteromedially in ventral view (Figure 4a). In rostral view (Figure 4c), it exhibits substantial ventral development, with a markedly convex profile. The cotyla quadratojugalis (Figure 4b) is broad and rounded, proportionally large in size, like in galliforms [13] (Supplementary Information), located anterodorsal to the condylus lateralis, and oriented lateroanteriorly.

The processus orbitalis is long, slightly curved medially and dorsally, and tapers to a point (Figure 4a,b,d–g). It is notably characterized by an apparent articulation with the processus basipterygoideus, resulting in a unique triple quadrate-pterygoid articulation among extant and fossil birds. Because the quadrate, pterygoid, palatine, and neurocranium are preserved in articulation and in their natural position, this feature is highly unlikely to be a taphonomic artefact produced by post-mortem bone displacement. In medial view (Figure 4d), a crest connects the processus orbitalis ventrally with the pterygoid condyle. Dorsal to this crest lies a deep, narrow fossa, where in *Asteriornis* and galloanserans in

general, the basiorbital foramen is located. The condylus pterygoideus is narrower and more anteromedially projected than the medial condyle (Figure 4c,d,f). The condylus medialis is relatively small and separated from the condylus pterygoideus by a narrow, deep fossa (Figure 4d).

In caudal view (Figure 4e), between the condylus lateralis and condylus medialis, and closer to the latter, there is an elongated lateromedial ridge-like structure, which is absent in *Asteriornis*.

5.1.4. Quadratojugal

The only remaining part of the jugal arch is the quadratojugal, which is articulated to the quadrate (Figure 4g). It does not appear to be broken, suggesting it was not fully fused to the jugal arch, as in *Ichthyornis* [33]. However, unlike *Ichthyornis*, it possesses a ventromedially directed process (Figure 4h,k), resulting in a triangular shape in lateral view. The quadratojugal lacks the processus squamosus like *Hesperornis*, whereas it is present in *Pterygornis* and *Archaeorhynchus* [34,35]. It has a rounded head (Figure 4j), the dorsal margin is straight (Figure 4i), and the medial facies is concave (Figure 4j).

5.1.5. Pterygoid

The pterygoid (Figure 5) exhibits a complex morphology in both its proximal and caudal ends, as well as along its main body. A system of three ridges or crests, also described in [36] divides the body into dorsomedial, dorsolateral, and ventromedial surfaces (Figure 5a–f). The longest crest is the crista dorsalis (Figura 5a,b), which extends from the rostromedial end of the processus basipterygoideus to its junction with the crest of the facies articularis quadratica (Figure 5a,b). The crista ventralis medialis (Figure 5d, new term) is less pronounced and runs from the ventral base of the processus articularis basipterygoideus of the pterygoid and the processus rostralis (topographically identified as such, *sensu* Benito et al., 2022 [36]). It disappears before reaching the ventromedial margin of the facies articularis quadratica (Figure 5d). The third crest is the crista ventralis lateralis (Figure 5e, new term), shorter in length and taller than the others. The crista ventralis lateralis is the only one visible in the available view of the pterygoid of *V. iaai* MACN-PV 19.748. It shows similar rostrocaudal extent (Figure 5g). In *V. geitononesos*, the crista ventralis lateralis continues with the processus articularis palatini (new term) of the pterygoid (Figure 5a,c,e), which is sharply keeled ventrally, and extends caudally. The processus articularis palatini appears to be broken in the MACN-PV 19.748 specimen (Figure 5g).

These three crests, which delimit three surfaces, impart a twisted appearance to the body and increase the available surface area in an otherwise relatively short pterygoid element. The process that articulates with the basipterygoid (Figure 5b,e) is long and projects dorsally from the pes pterygoidei, rather than forming an elongate, flat surface as in Galloanseres. This morphology is particular to Aves. In *V. iaai* MACN-PV 19748, this process is broken, and only the base is preserved (Figure 5g).

The facies articularis palatina, at the anterior end of the pterygoid, is concave and bears a foramen within a deep depression (Figure 5c). The facies articularis basipterygoideus is located medial to the facies articularis palatina, at the anterior end of the pterygoid (Figure 5e,i,j), as in Galloanseres. It is ovoid (although its dorsal and ventral ends curve anteriorly) and slightly concave. It is small relative to the pes pterygoidei (Figure 5b) and is separated from it, forming a dorsal process. Anterior and ventral to the facies articularis basipterygoideus, there is a processus rostralis that articulates medially and ventrally with the palatine, and dorsally with the rostrum parasphenoidale (Figure 5c,d,i), at the rostral end of the processus basipterygoideus. The processus rostralis is relatively long

and slightly twisted, which may represent an autapomorphy of *Vegavis* (Figure 5b,e,g). This is the unique process preserved in *V. iaai* MACN-PV 19.748 (Figure 5g), and it is more robust than the processus rostralis of *V. geitononesos*. *Puffinus puffinus* and *Gavia arctica* possess a recurved "rostral process", although much shorter and less robust than that of *V. geitononesos* and *V. iaai*. *Anas plathyrinchos*, *Biziura lobata* and *Mergellus albellus* have a very long rostral process, weakly twisted or nearly straight, and spine-like in shape.

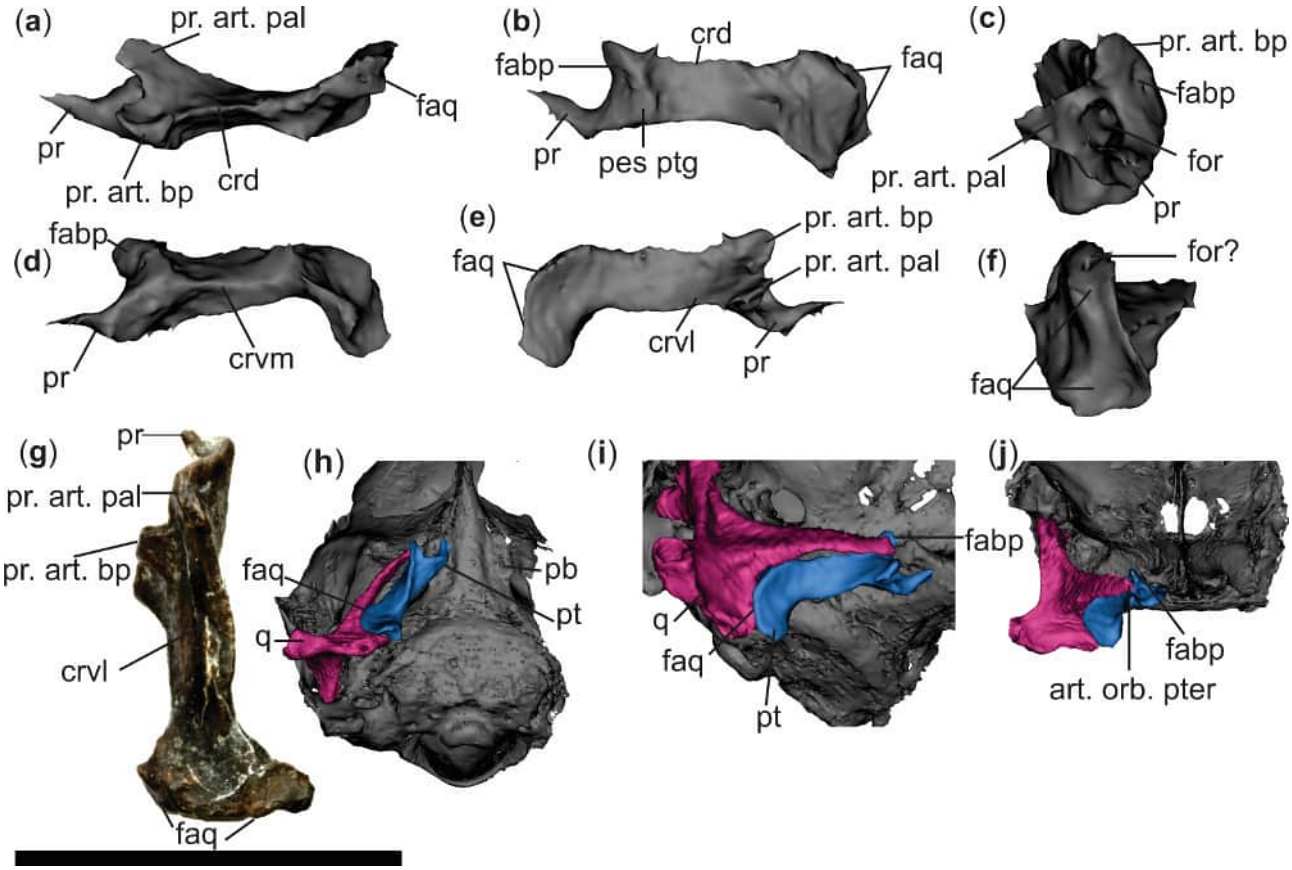

Figure 5. Pterygoid, quadrate, and cranium of *V. geitononesos* sp. nov. (MLP-Pv 15-I-7-52) compared with the pterygoid of *V. iaai* (MACN-Pv 19.748). Right pterygoid of *V. geitononesos* in (**a**) dorsal, (**b**) medial, (**c**), rostral, (**d**) ventral, (**e**) lateral, and (**f**) caudal views. Left pterygoid of *V. iaai* (digitally removed from sedimentary matrix) in (**g**), ventral view. Cranium, quadrate, and pterygoid of *V. geitononesos* articulated in (**h**) ventral, (**i**), ventrolateral, and (**j**) rostral views. Abbreviations: art. orb. pter, articulation of processus orbitalis with processus articularis basipterygoideus; crvl, crista ventralis lateralis; pr, processus rostralis; crd, crista dorsalis; crvm, crista ventralis medialis; fabp, facies articularis basipterygoidei; faq, facies articularis quadratica; for?, foramen?; q, quadrate; pb, processus basipterygoideus; pes ptg, pes pterygoidei; pr. art. bp, processus articularis basipterygoideus; pr. art. pal, processus articularis palatinus; pt, pterygoid. ((**h**–**j**) not to scale). Scale bar = 10 mm.

At the caudal end, the wide facies articularis quadratica (Figure 5f) acquires a convex and fan-shaped wing that laterally covers the quadrate (Figure 5b,e,i), like in *V. iaai* MACN-Pv 19.748. The articulation with the quadrate (Figure 5h–j) is double, involving the condylus pterygoideus and the processus orbitalis. The pterygoid is largely similar to that of *V. iaai* MACN-PV 19.748 (Figure 5g), but smaller.

5.1.6. Palatinum

The posterior half of the right palatinum (Figure 6) is preserved in articulation with the pterygoideum and rostrum parasphenoidale. The medial margin is convex, whereas the lateral margin is concave, giving the element an overall fan-shaped appearance (Figure 6a,b,h). This morphology is uncommon among Neornithes but shared with juveniles of *Spheniscus* and *Aptenodytes*, as well as with *Madrynornis* [37,38] and *Macronectes*. The pars lateralis (Figure 6a–c,f) expands lateroanteriorly, whereas the pars choanalis (Figure 6a,c,d), which is smaller in surface area than the pars lateralis, projects dorsomedially. The caudal palatine of *V. notopothousa* AMNH FARB 30899 is very poorly preserved, with the pars choanalis and the rostral portion of pars lateralis being the comparable section. Like *V. geitononesos*, the pars choanalis projects dorsomedially, while the pars lateralis appears to have a concave lateral margin. The crista ventralis is low, separating the pars choanalis from the pars lateralis. The fossa ventralis palatina (Figure 6a) is nearly flat. The lateral margin (Figure 6e,g) is concave, not developing a true crista lateralis. The medial margin of the pars choanalis forms a crista medialis that is medially convex (Figure 6c). The pars lateralis is positioned more ventrally than the pars choanalis, and together they form an obtuse angle (Figure 6g–i). On the dorsal surface, a low crista dorsalis extends obliquely from the processus pterygoideus to the medial margin, delimiting two dorsal surfaces (Figure 6b). The processus pterygoideus is lateral and hook-shaped, projecting medially. The palatine–pterygoid articulation is of the ball-and-socket type (Figure 6h,i).

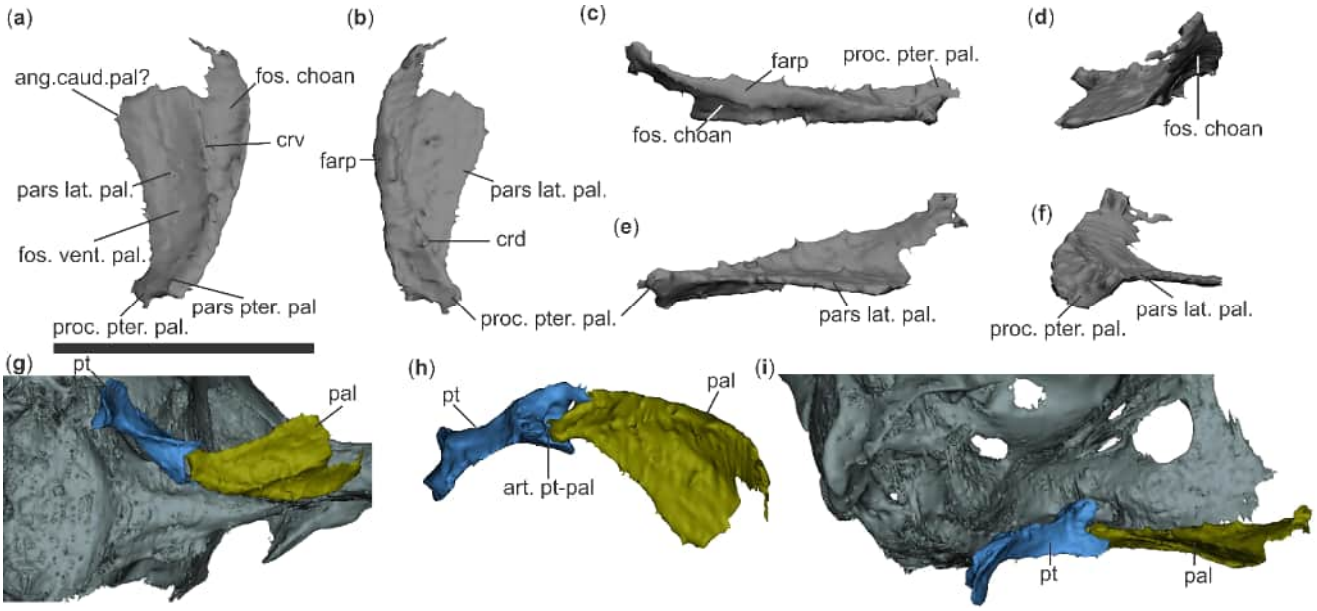

Figure 6. Palatine, pterygoid, and cranium of *V. geitononesos* sp. nov. (MLP-Pv 15-I-7-52). Right palatine in (**a**) ventral, (**b**) dorsal, (**c**) medial, (**d**) rostral, (**e**) lateral, and (**f**) caudal views. Cranium, pterygoid, and palatine articulated in (**g**) ventral and (**i**) lateral views. Palatine and pterygoid articulated in (**h**) dorsorostral view. Abbreviations: ang. caud. pal?, angulus caudolateralis palatini; art. pt-pal, articulatio pterygopalatina; crd, crista dorsalis palatini; crv, crista ventralis; farp, facies articularis parasphenoidalis; fos. choan, fossae choanalis; fos. vent. pal., fossae ventralis palatinum; pal, palatinum; pars lat. pal., pars lateralis palatini; pars pter. pal., pars pterygoideus palatini; proc. pter. pal., processus pterygoideus palatini; pt, pterygoid. ((**g**–**i**) not to scale). Scale bar = 10 mm.

5.1.7. Mandible

Both mandibular rami are complete, except for the mandibular symphysis (Figure 7). There is no evidence of the intraramal mandibular joint inferred for *V. iaai* and *V. notopothousa* AMNH FARB 30899 [8] based on the taphonomic fractures observed in the

reconstructions of the materials. In caudal view (Figure 7m), a deep, triangular fossa caudalis faces caudally and is markedly similar to that of *V. iaai* MACN-Pv 19.748. On the contrary, the fossa caudalis of *V. notopothousa* is poorly preserved, and more dorsally oriented. Related to that, the "processus retroarticularis" (identified as the caudalmost portion protruding from the mandible) is short and projects ventrolaterally (Figure 7a,b), as in *V. iaai* MACN-Pv 19.748, whereas in *V. notopothousa* it points caudoventrally and is more horizontal.

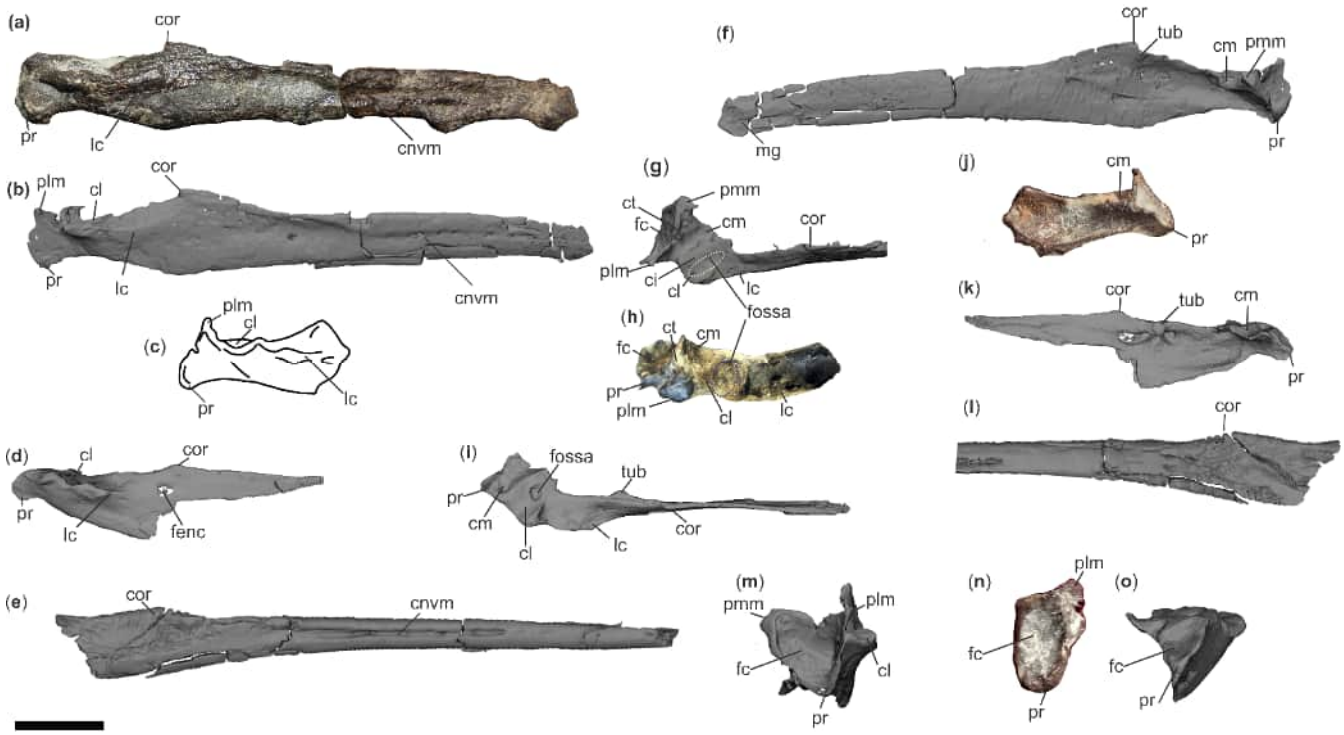

Figure 7. Specimen and virtual reconstruction of the mandible of *V. geitononesos* sp. nov. (MLP-PV 15-I-7-52), compared with other Cretaceous Antarctic birds. Mandible of *V. geitononesos* in (**a**), (**b**) right lateral view, (**f**) medial view, (**g**) dorsal view, (**m**) caudal view. *V. iaai* (MACN-Pv 19.748) in (**c**) lateral view (drawing from Álvarez Herrera et al., 2024 [5]), (**h**) dorsal view, (**j**) medial view, (**n**) caudal view. *V. notopothousa* sp. nov. AMNH FARB 30899 (mirrored) in (**d**) lateral view, (**i**) dorsal view (**k**) medial view, and (**o**) caudal view. *Pujatopouli soberana* in (**e**) lateral view, (**l**) medial view. Abbreviations: ci, crista intercotylaris; cl, cotyla lateralis; cm, cotyla medialis; cnvm; canalis neurovascularis mandibularis; cor, "processus coronoideus"; ct, crista transversa; fc, fossa caudalis; fenc, fenestra caudalis; plm, processus lateralis mandibulae; pmm, processus medialis mandibulae; pr, processus retroarticularis; tub, tuberculum. Scale bar = 10 mm.

The processus medialis mandibulae is as tall as the dorsal end of the crista transversa fossae (Figure 7f,m). The latter is straight and high, resembling *V. iaai* MACN-Pv 19.748 (not preserved in *V. notopothousa* AMNH FARB 30899). The processus lateralis mandibulae is thin (Figure 7j,m), whereas it is wider and forms a tubercle in *V. iaai* MACN 19.748.

The cotyla medialis is elongated, oriented anteromedially–posterolaterally and separated from the cotyla lateralis by a low but well-defined crista intercotylaris (Figure 7j). This condition is similar in *V. notopothousa* AMNH FARB 30899 (Figure 7l), whereas in *Vegavis* MACN-Pv 19.748, the crista intercotylaris is lower.

Within the cotyla lateralis, there is an oval fossa medially located, which is also present in *V. iaai* MACN-Pv 19.748 and *V. notopothousa* AMNH FARB 30899 (Figure 7j–l). In *V. iaai* MACN-Pv 19.748, the cotyla lateralis is broader than in the other species proposed here for *Vegavis*.

In lateral view, the robust lateral crest (sensu Álvarez Herrera et al., 2024) [5] extends rostrally and reaches the "processus coronoideus" (in the sense of mandibular apex). In other species of the genus, the lateral crest likewise extends rostrally, but with a different extension. In *V. notopothousa* AMNH FARB 30899 (Figure 7i), it extends to the level of the tuberculum mediale, whereas in *V. iaai* MACN-Pv 19.748 the extension is more limited, terminating at a small lateral fossa (Figure 7c,d). The "processus coronoideus" and the fenestra caudalis mandibularis are nearly aligned in *V. notopothousa* AMNH FARB 30899, with the "processus coronoideus" positioned slightly more rostrally (Figure 7d). In *Pujatopouli* and *V. geitononesos*, no fenestrae are observed (Figure 7a,b,e,i).

The ventral margin of the articular region is concave in *V. geitononesos* MLP-Pv 15-I-7-52 and *V. iaai* MACN-Pv 19.748 (although in the latter it appears partially eroded, particularly along the medial edge of the ventral margin). In contrast, it is convex in *V. notopothousa* AMNH FARB 30899 (Figure 7b–d). In lateral view, the processus retroarticularis is separated from the ramus mandibulae through a concave ventral margin, more expanded in *V. geitononesos* MLP-PV 15-I-7-52 and *V. iaai* MACN-Pv 19.748 and shorter in *V. notopothousa* AMNH FARB 30899, in which it forms a deeper notch (Figure 7a–d,f–h).

In medial view, the mandible of *V. geitononesos* MLP-PV 15-I-7-52 shows a concave surface extending from the "processus coronoideus" to the anteroventral end of the fossa caudalis (Figure 7f), as in *Vegavis* MACN-Pv 19.748. In contrast, in *V. notopothousa* AMNH FARB 30899, the concavity is truncated at the level of the condylus medialis (Figure 7g,h).

The "processus coronoideus" is well developed and higher (Figure 7a) than that of *V. notopothousa* AMNH FARB 30899. Immediately posterior to this process, there is a small tuberculum pseudotemporale, which is much less robust than that of *V. notopothousa* AMNH FARB 30899, not preserved in *V. iaai* MACN-Pv 19.748 (Figure 7f–i), and is absent in *Pujatopouli* [14].

On the lateral side of the mandible, there is a canalis neurovascularis mandibularis (Figure 7a,b), as in *V. notopothousa* AMNH FARB 30899 and *Pujatopouli* (Figure 7d,e). Within the canalis neurovascularis mandibularis a series of large foramina open, as in *Pujatopouli*. Near the mandibular symphysis, which is broken, there is a medial groove close to the ventral margin (Figure 7f), as in *Pujatopouli*. The rami mandibulare are more robust and higher than in *Pujatopouli* (Figure 7a,e). The rostrum mandibulare is slightly ventrally curved (Figure 7b), unlike the dorsal curvature observed in *V. notopothousa* AMNH FARB 30899 and the straight symphysis of *Pujatopouli*.

5.1.8. Cervical Vertebra Indet

The vertebra (Figure 8) is a posterior cervical, probably the C10. It is almost as long as tall, and it does not preserve the zygapophysis cranialis. The processus spinosus is slightly caudally projected (Figure 8c,e). The facies articularis cranialis is heterocoelous (Figure 8a). On the right lateral side (Figure 8d), there is a well-developed processus costalis, directed ventrocaudally, which delimits the foramen transversarium. In lateral view (Figure 8c,d), a dorsoventrally high lamina arcocostalis is visible. In ventral view (Figure 8f), anterior to the facies articularis cranialis, there is a deep fossa, oval in shape transverse to the corpus vertebrae. The processus ventralis (Figure 8a,f) is well developed, forming a narrow lamina that projects caudally.

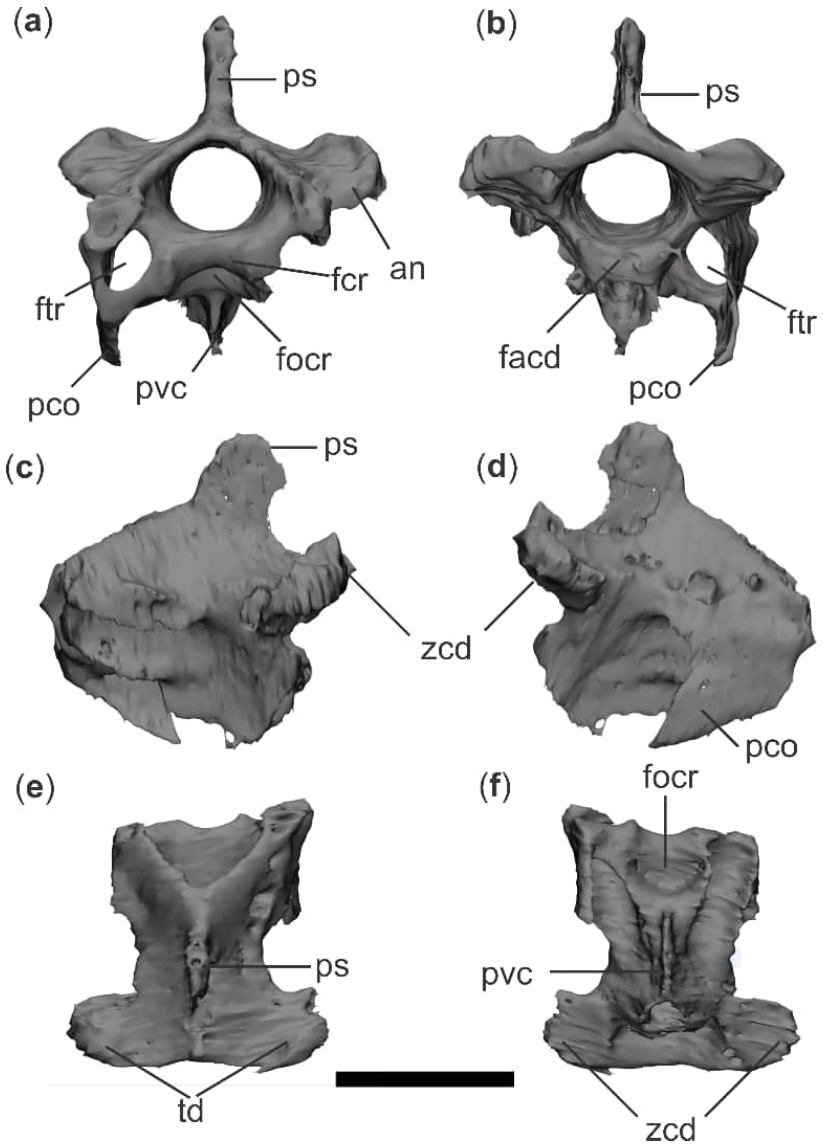

Figure 8. Virtual reconstruction of posterior cervical vertebra of *V. geitononesos* sp. nov. (MLP-PV 15-I-7-52). Vertebra in (**a**) rostral, (**b**) caudal, (**c**) left lateral, (**d**) right lateral, (**e**) dorsal and (**f**) ventral views. Abbreviations: an, ansa costotransversaria; facd, facies articularis caudalis; fcr, facies articularis rostralis; focr, fossae cranialis; ftr, fenestrae transversaria; pco, processus costalis; ps, processus spinosus; pvc, processus ventralis corporis; td, torus dorsalis; zcd; zygapophysis caudalis. Scale bar = 10 mm.

5.1.9. Pelvis

The os coxae (Figure 9a–d), although highly incomplete, preserves elements permitting comparison with *Vegavis iaai* MLP-PV 93-I-3-1 (Figure 9h) and *Pujatopouli* (Figure 9k,l). The ala preacetabularis ilii (Figure 9a,b,i,j) is small, gracile, and oval-shaped. Its ventral margin is markedly concave, while the dorsal surface of the preserved portion of the ala preacetabularis ilii is convex.

The acetabulum (Figure 9a,c) is large and, although its dorsal portion and the antitrochanter are not preserved, is distinctly circular. A weak tuberculum preacetabulare lies anteroventral to the acetabulum, as in *Pujatopouli* (Figure 9k,l) and *V. iaai* (Figure 9h), although more similar to the former. The ratio between acetabular size and ala preacetabularis ilii size is greater in *V. geitononesos* MLP-PV 15-I-7-52 than in *Vegavis iaai* and *Pujatopouli* (see also [4] and Figure 3D,E in [14]).

The ischium preserves part of the corpus ischii (Figure 9a). Posterior to the corpus lies the anteriormost section of the ala ischii. Ventral to the ischium is the anterior portion of the pubis, which is slightly compressed lateromedially and rotated posteriorly in a dorsolateral direction.

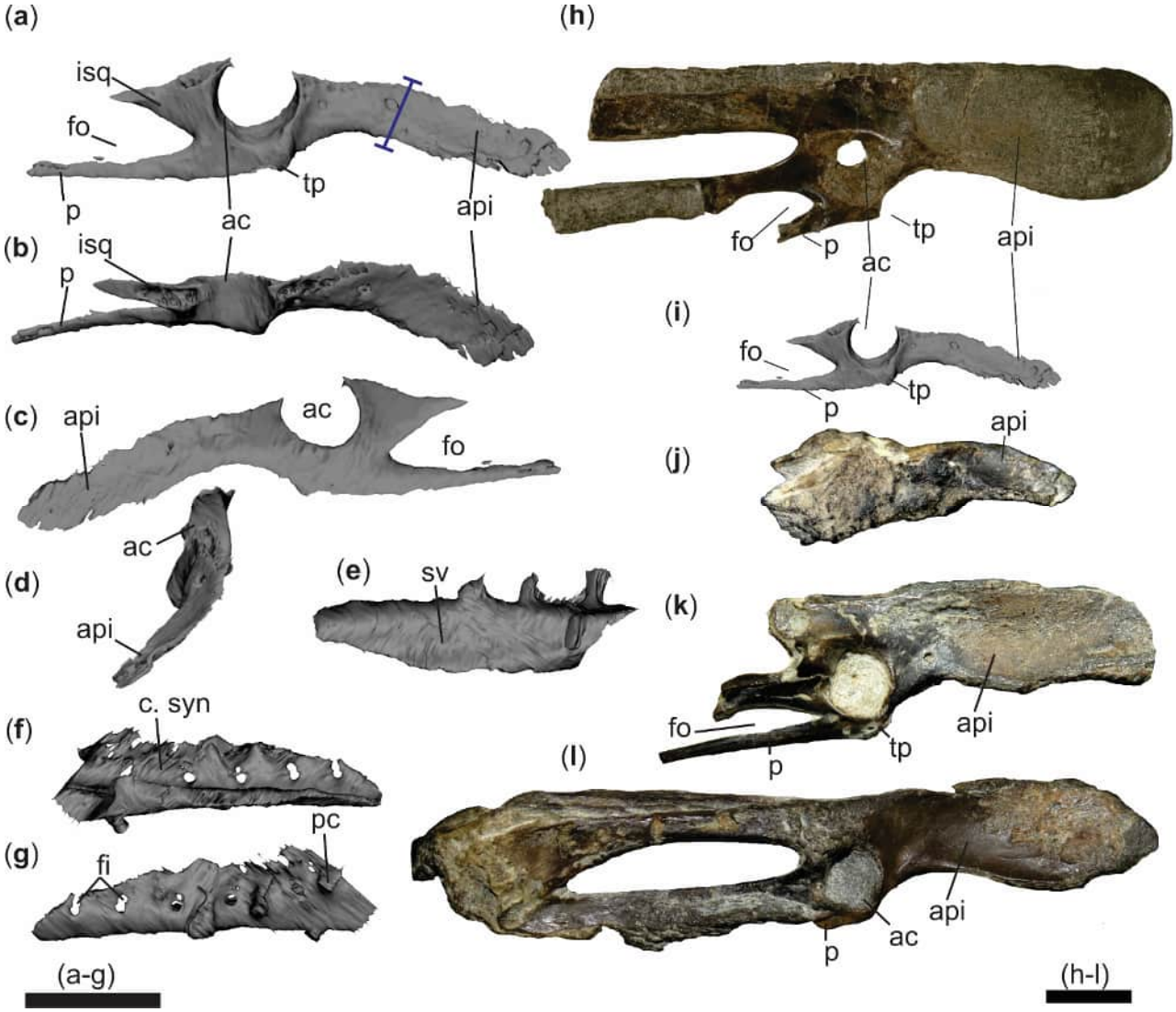

Figure 9. Ossa coxae and synsacrum of *V. geitononesos* sp. nov. (MLP-PV 15-I-7-52) compared with *V. iaai* and *Pujatopouli*. Virtual reconstruction of the ossa coxae of *V. geitononesos* in (**a**) lateral, (**b**) dorsal, (**c**) medial, and (**d**) rostral views. Fragment of synsacrum (virtual reconstruction) of *V. geitononesos* in (**e**) ventral, (**f**) medial, and (**g**) lateral views. Ossae coxae comparisons in lateral view of (**h**), *V. iaai* (holotype MLP-PV 93-I-3-1), (**i**,**j**), *V. geitononesos*, and (**k**,**l**) *Pujatopouli soberana*. Abbreviations: ac, acetabulum; api, ala preacetabularis ilii; c. syn, canalis synsacralis; fi, foramina intervertebralia; fo, foramen obturator; isq, ischium; p, pubis; pc, processus costalis; sv, sulcus ventralis; tp, tubercula preacetabularia. The blue lines in (**a**) demarcate the portion of the ilium where the preacetabular iliac crest is preserved. Scale bar = 10 mm.

Together, the pubis and ischium delineate the anterior margin of the foramen obturatum (Figure 9a,c,i). This opening is relatively taller than in *Pujatopouli* (Figure 9k) and exhibits a sharp anterior margin, though less pronounced than in *Pujatopouli*, whereas in *Vegavis* (Figure 9h) the margin is rounded.

5.1.10. Synsacrum

The synsacrum (Figure 9e–g) is incomplete and exhibits at least six fused vertebrae. The five corresponding intervertebral foramina are figure of eight (Figure 9f,g), unlike those in *Pujatopouli* and *V. iaai* MLP-PV 93-I-3-1, which are more circular or oval. We found arrangements of these foramina in pairs in some falconiforms, pelecaniforms, and procellariiforms, but none with this shape. On the right lateral side, there are three processes: the two cranial ones correspond to the processus transversus, which is developed anterodorsally (Figure 9g). The third one is the processus costalis, which projects ventrally onto the ventral facies of the synsacrum and is more robust than in *Pujatopouli*, where the process projects laterally. This vertebra articulates with the pelvis at the acetabular level, allowing it to be identified as a sacral vertebra, more specifically, the vertebra acetabularis.

5.1.11. Femur

The right femur (Figure 10d,h–k,o,s–v) exhibits a lateromedially curved shaft (Figure 10o,s), as in *Vegavis iaai* (Figure 10m,n,r,s), and *Polarornis* (Figure 10l–p). Its distolateral margin presents a highly developed crista intermuscularis, elongated in a proximocaudal direction, unlike the condition in *Vegavis iaai* MLP-PV 93-I-3-1, MACN-Pv 19.748, and *Polarornis*.

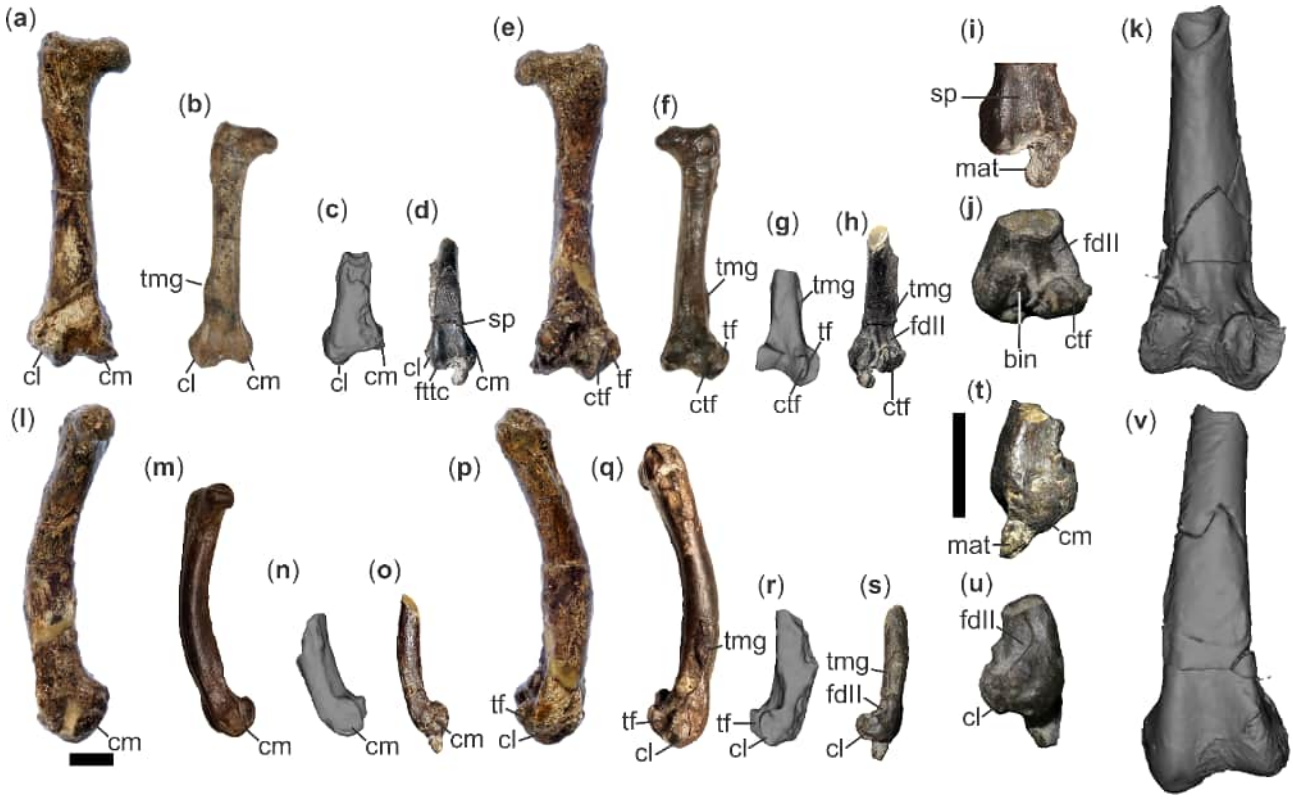

Figure 10. Femur comparisons (specimens and virtual reconstructions). *Polarornis gregorii* in (**a**) cranial, (**e**) caudal, (**l**) medial, and (**p**) lateral views. *Vegavis iaai* (MACN-Pv 19.748) in (**b**) cranial, (**f**) caudal, (**m**) medial, and (**q**) lateral views. *V. iaai* (MLP-PV 93-I-3-1) in (**c**) cranial, (**g**) caudal, (**n**) medial, and (**r**) lateral views. *V. geitononesos* sp. nov. (specimen) in (**d**) cranial, (**h**) caudal, (**o**) medial, and (**s**) lateral views; detail of distal femur in (**i**) cranial, (**j**) caudal, (**t**) medial, and (**u**) lateral views. *V. geitononesos* (virtual reconstructions, with sedimentary matrix removed) in (**k**) caudal and (**v**) caudal views. Abbreviations: bin, bone indet.; cl, condylus lateralis; cm, condylus medialis; ctf, cristae tibiofibularis; fdII, insertion of flexor perforatus digiti II; fttc, fovea tendineus musculi tibialis cranialis; mat, sedimentary matrix; sp, sulcus patellaris; tf, trochlea fibularis; tmg, tuberculum musculus gastrocnemialis. (**k**,**v**) not to scale. Scale bar = 10 mm.

The tuberculum musculus gastrocnemialis is less prominent than in *V. iaai*, particularly regarding specimen MAC-Pv 19.748, in which the scar is longitudinally extended (Figure 10b–d,v). In *V. iaai* MLP-PV 93-I-3-1, this scar is not well preserved.

In cranial view, the patellar sulcus is deeper and narrower than in *V. iaai* MLP-PV 93-I-3-1 and is bounded by two subparallel ridges (Figure 10d). This contrasts with *V. iaai* (both MLP-PV 93-I-3-1 and MACN-Pv 19.748 specimens), where the medial and lateral condylar ridges diverge distally (Figure 10b,c).

The condylus lateralis projects distolaterally, as in *V. iaai* MLP-Pv 93-I-3-1 and MACN-Pv 19.748 and *Polarornis*, though to a much lesser degree (Figure 10f–k). Regarding distal extension, in anterior view the lateral condyle exceeds the condylus medialis by less than half its length (Figure 10d), more closely resembling *V. iaai* MACN-PV 19.748 (Figure 10b) than MLP-PV 93-I-3-1 specimen (Figure 10c).

The trochlea fibularis is broad, delimited by a crista fibularis nearly equal in extent to the crista tibiofibularis (Figure 10h,j,k), unlike *V. iaai* MLP-PV 93-I-3-1 (Figure 10g), where the crista fibularis is larger. The anterolaterally oriented fossa, located proximal to the trochlea fibularis and medial to the epicondylus lateralis (Figure 10h,j–k), is similar to, but deeper than, that of *V. iaai* MLP-PV 93-I-3-1. The fossa poplitea is shallow and restricted to a small subtriangular space.

5.1.12. Tarsometatarsus

The proximal half of the left tarsometatarsus (Figure 11) is well-preserved, except for the margins of the articular cotylae, and is still partially covered by sediment. The proximal end presents two well-defined cotylae; the area of the cotyla lateralis being smaller than that of the cotyla medialis (Figure 11b,k). The cotyla medialis (Figure 11b) is elongated in a dorsoplantar direction and is bounded laterally and medially by two ridges. The cotyla lateralis is rounded, shallower, and less extended proximally than the cotyla medialis, and delimited by a low medial ridge (Figure 11k). Only the base of the eminentia intercotylaris is preserved.

The sulcus extensorius is deep and wide (Figure 11d), unlike in *V. iaai*, in which it is deep but narrows distally (Figure 11f). Both cristae dorsalis lateralis et medialis delimit this sulcus, and unlike *V. iaai*, the crista medialis is low and broad (Figure 11d,f). Both foramina vascularia proximalia are similarly sized, like in *V. iaai* (Figure 7d,e). The foramen vasculare proximale laterale is slightly more proximal than the foramen vasculare proximale mediale and partially overlaps it (Figure 11e). On the contrary, in *V. iaai*, the foramen vasculare proximale laterale is slightly more distally located than the foramen vasculare proximale mediale.

The shaft is rounded (Figure 11h), unlike in *V. iaai*, where it is strongly lateromedially compressed. The facies medialis of *V. geitononesos* is convex (Figure 11i), whereas it is flat in *V. iaai*. The tuberositas m. tibialis cranialis consists of two blunt protuberances centered within the sulcus extensorius (Figure 11d). The proximal protuberance is elongated, and the distal one is rounded. Both protuberances are distal to the foramina vascularia proximalia in *V. geitononesos*, whereas in *V. iaai*, the tuberositas are in-between the foramina.

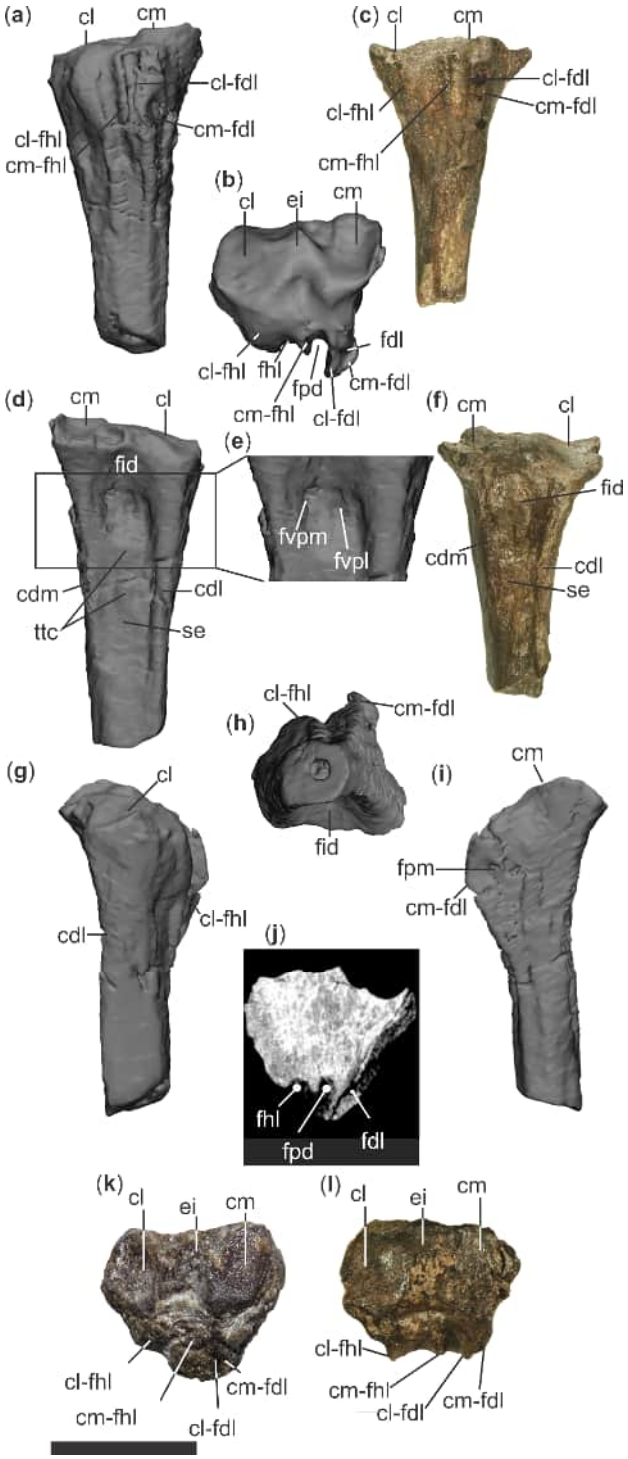

Figure 11. Virtual reconstructions and tarsometatarsus specimen of *Vegavis geitononesos* sp. nov. (MLP-Pv 15-I-7-52) in (**a**) plantar, (**b**,**k**) proximal, (**d**,**e**) dorsal, (**g**) lateral, (**h**) distal, (**i**) medial, and (**j**) CT image of cross-section at the hypotarsal level in proximal views. *Vegavis iaai* (holotype MLP-PV 93-I-3-1, mirrored) in (**c**) plantar, (**f**) dorsal, and (**l**) proximal views. Abbreviations: cdl, crista dorsalis lateralis; cl, cotyla lateralis; cl-fdl, crista lateralis flexor digitorum longus; cl-fhl, crista lateralis flexor hallucis longus; cm, cotyla medialis; cdm, crista dorsalis medialis; cm-fdl, crista medialis flexor digitorum longus; cm-fhl, crista medialis flexor hallucis longus; ei, eminentia intercotylaris; fdl, canal of the flexor digitorum longus; fhl, canal of the flexor hallucis longus; fid, fossa infracotylaris dorsalis; fpd, sulcus for the flexor perforans digiti 2; fpm, foramen proximale mediale; fvpl, foramen vasculare proximale laterale; fvpm, foramen vasculare proximale mediale; se, sulcus extensorius; ttc, tuberositas tibialis cranialis. Scale bar = 10 mm.

The hypotarsus comprises four well-developed crests that delimit two clearly differentiated sulci and a closed canal (Figure 11a,b,j), as in stem-Gaviiformes, Palaelodidae (Phoenicopteriformes), Alcidae (Charadriiformes), and Anatidae (Anseriformes) [19]. In *V. geitononesos*, these crests extend further distally along the facies caudalis, whereas in *V. iaai*, the hypotarsus is more proximally restricted. The crista lateralis and crista medialis, enclosing the canal for the flexor digitorum longus tendon (Figure 11a,b), are the most plantarly developed. This canal has not been described for *V. iaai* MLP-PV 93-I-3-1, in which only the bases of these two crests are preserved (Figure 11c,l). The state of preservation of the hypotarsal crests of *V. iaai* does not allow the exclusion of a fully developed canal for the flexor digitorum longus tendon, but at present this structure can only be observed in *V. geitononesos*. The crista medialis and crista lateralis for the flexor hallucis longus are well-separated, leaving a wide sulcus between them (Figure 11a,c,j). The shape of the cl (fhl) can be misleading, at some heights it appears as a broad, rounded crest (Figure 11a–c), whereas at others, the plantar end appears flattened, giving rise to two subcrests. The cl (fhl) is small and less extended in *V. iaai*. Between the cm (fhl) and the cl (fdl) lies a deep sulcus that housed the flexor perforatus digiti II tendon (Figure 11a,b,j), which is slightly shallower in *V. iaai*. On the medial side of the hypotarsus is the foramen plantare proximale (Figure 11i), which opens medially to the cm (fdl). In *V. geitononesos*, the cm–fhl, cm–fdl, and cl–fdl converge distally, forming a crest that runs longitudinally and parallel to the cl–fhl, whereas in *V. iaai* these crests are less extensively developed on the facies plantaris.

6. Discussion

Several possible scenarios were evaluated before proposing a new species to account for the similarities and differences between MLP-PV 15-I-7-52, the holotype of *Vegavis geitononesos*, and *V. iaai*. The main differences observed are discussed in relation to ontogenetic variation and sexual dimorphism, which are potential sources of variation based on observations in other birds. The possible role of taphonomic processes is also considered.

6.1. Ontogenetic Maturity

Skeletal morphology does not remain static after hatching but changes progressively as individuals grow and approach adulthood [39]. Juvenile birds are commonly characterized by limited mineralization and a relatively porous cortex [40], persistent sutures in both cranial and postcranial regions [39], and little or no fusion in compound elements such as the synsacrum or carpometacarpus [18]. In contrast, mature individuals exhibit a higher degree of ossification throughout the skeleton, progressive closure of sutures (particularly in the skull [41–43]), increased bone compactness [44], and extensive fusion of elements of the axial and appendicular skeleton [18,39]. These developmental modifications are not uniform across the skeleton [45,46] nor among taxa [45,47–49], and their timing reflects both phylogenetic constraints and life-history patterns, including the onset of functional independence and reproduction [39,44]. As a result, individuals of the same species at different ontogenetic stages may display noticeable differences in size, proportions, and robustness, some of which may superficially resemble taxonomic or sexual variation. However, their ontogenetic origin can often be readily assessed.

In aquatic birds such as penguins, skeletal ontogeny is further shaped by the mechanical and functional requirements of swimming and diving [50]. *Vegavis* probably exhibits a similar condition, given its inferred diving habit [4]. During growth, long bones tend to become more robust, cortical thickness increases, and structural reinforcement becomes more pronounced, contributing to a more rigid skeleton capable of withstanding hydrodynamic forces [51,52]. In diving taxa, these changes may include enhanced bone compactness or osteosclerosis, which is associated with decreased buoyancy [53,54] and

improved underwater stability [44,55]. Ontogenetic differences in this kind can therefore generate substantial intraspecific morphological variability in aquatic birds, highlighting the importance of considering developmental stage when interpreting anatomical differences in both extant and fossil forms.

The specimen MLP-PV 15-I-7-52 can be evaluated using some of the criteria proposed by Griffin et al. (2021) [56] and Tumarkin-Deratzian et al. (2006) [40] and subsequently applied to numerous other birds to assess ontogenetic maturity. The skull of MLP-PV 15-I-7-52 exhibits complete ossification, with no visible sutures, as does the mandible. The femoral surface of MLP-PV 15-I-7-52 lacks porosity or striations that produce rough surface textures associated with active periosteal ossification, typically expected in juvenile stages. Instead, it is smooth as in mature birds due to cessation of circumferential bone growth [40,48]. Furthermore, ossification centers of the femoral articular regions have been documented across different ontogenetic stages [49], but only in adult individuals is the distal end, including the condylar region, reported as fully ossified [57] as in MLP-PV 15-I-7-52.

In summary, the smooth texture of all bones, the absence of visible sutures in the preserved elements, and the complete ossification and fusion of the femoral end together provide strong evidence supporting the adult status of MLP-PV 15-I-7-52. Consequently, the morphological differences observed between this specimen and *Vegavis iaai* are unlikely to result from ontogenetic variation.

6.2. Sexual Dimorphism

Sexual differences in the avian skeleton may be expressed through variation in size, relative proportions, and bone robustness, as well as in the configuration of specific regions such as the pelvis and long bones [58]. Dimorphism in body size is common in many extant bird species, including members of Anseriformes [59,60] and Aequornithes [61], in which males are usually larger than females. Other features, such as the size of the acetabular region, have been reported as sexually dimorphic, being larger in females than in males as a consequence of pelvic modifications associated with reproduction and the need to accommodate egg passage [59]. In other cases, dimorphism affects particular elements of the skeleton, such as the third toe and bill length, which are larger in male penguins [62], as well as overall skeletal proportions, with males usually being larger [61,63–65].

MLP-PV 15-I-7-52 exhibits a set of differences relative to *V. iaai* (MLP-PV 93-I-3-1 and MACNPV 19.748), including a different configuration of the hypotarsal crests, the mediolateral compression of the tarsometatarsal shaft, the divergence and extension of the femoral condyle, and a pelvis with more gracile ala preacetabularis ilii and a relatively larger acetabulum. Assuming that the three specimens (MLP-PV 93-I-3-1, MACNPV 19.748, and the new MLP-PV 15-I-7-52) could belong to the same species, the morphological evidence could be interpreted in terms of sexual dimorphism as follows. The larger size of the tarsometatarsus and mandible observed in the new specimen suggests that it represents a male, although other parameters must be evaluated [48]. However, pelvic morphology, particularly the acetabular size, indicates the opposite, being more consistent with a female condition, in which the acetabular region is usually larger than in males [59], and even the acetabulum is frequently wider in females [66], (Table 1).

Table 1. Estimation of body masses in Antarctic specimens, with minimum and maximum values according to estimated error.

Taxa	Element	Estimator (Author)	BM	Min BM	Max BM
Polarornis gregorii	Femur (1)	Circumference [20],	2820 g	1895 g	3745 g
Pujatopouli soberana	Humerus	Circumference	2030 g	1454 g	2606 g
Vegavis iaai MLP-PV 93-I-3-1	Femur	Circumference [20],	1189 g	799 g	1579 g
V. iaai MLP-PV 93-I-3-1	coracoid	Faceta humeralis [20],	1180 g	1027 g	1333 g
V. geitononesos MLP-PV 15-I-7-52	Femur	Circumference [20],	696 g	468 g	924 g
Antarcticavis capelambensis	Femur	Circumference [20],	870 g	623 g	1117 g
Conflicto antarcticus	Femur	Circumference [20],	1642 g	1102 g	2178 g

1. Estimated using the diameters in section.

Although the evidence is limited, the new specimen described here shows contradictory patterns. The two previously published *Vegavis iaai* skeletons, the holotype (MLP-PV 93-I-3-1) and the second skeleton (MACN-Pv 19.748), differ slightly in size, which could be attributable to either individual variation or to sexual dimorphism. In contrast, evidence from the new specimen MLP-PV 15-I-7-52 is inconsistent with a simple interpretation in terms of sexual dimorphism, at least until further evidence becomes available.

6.3. Taxonomic Differences

A set of similarities and differences has been identified among specimens previously referred to *Vegavis iaai* and the new skeleton described here. Ontogenetic variation and sexual dimorphism are excluded as plausible explanations for the entirety of the observed morphological disparity (see Sections 6.1 and 6.2). On this basis, the available anatomical evidence supports the recognition of three species within the genus *Vegavis*.

The type species, *V. iaai*, is consequently represented by the holotype MLP-PV 93-I-3-1 and the specimen MACN-Pv 19.748, which differ primarily in size. These differences are interpreted as intraspecific variation, potentially related to sexual dimorphism. In contrast, the differences observed between the new specimen MLP-PV 15-I-7-52 and the previously described specimen AMNH FARB 30899 [6] exceed the expected range and nature of intraspecific variation and are proposed as two new species.

The specimen MLP-PV 15-I-7-52 is therefore proposed as the holotype of *Vegavis geitononesos* sp. nov. Its assignment to *Vegavis* is supported by a set of characters of the skull, femur, and tarsometatarsus, as listed in the amended diagnosis of the genus (see Section 4.1), and indicated with an asterisk. Unique features are included in the specific diagnosis above and involve characters of the skull, synsacrum, pelvis, femur, and tarsometatarsus (Section 4.1.3).

Finally, the skull AMNH FARB 30899 is proposed as the holotype of *Vegavis notopothousa* sp. nov. Its generic assignment is supported by the configuration of the pterygoid and the mandible [6]. Nevertheless, the numerous characters listed in its diagnosis (Section 4.2) support its recognition as a distinct species

6.4. Insights from Vegavis into Neognathous Palate Evolution

The neognathous palate type has been proposed as plesiomorphic for Neornithes, based on the description of the palatine and pterygoid in Ichthyornithes [36]. However, the fossil record of these elements is very limited in Cretaceous Neornithes, with a nearly complete pterygoid reported for *V. iaai* (MACN-Pv 19.748) and the maxillary process of the palatine for *Polarornis* [67] and *V. notopothousa* sp. nov. [6]. The specimen described here represents the first record of the quadrate, pterygoid, and palatines preserved in

articulation with one another and with the neurocranium, providing a unique opportunity to analyze the palate in a Cretaceous neornithine bird such as *Vegavis*.

The arthrology of the elements involved in cranial kinesis shows a quadrate articulated to the neurocranium by two well-differentiated condyles, a condition that has been recovered as an apomorphy of Neognathae [13,68]. The quadrate articulates with the caudal pterygoid through a double joint, involving a condylus pterygoideus and an articular surface at the base of the processus orbitalis. This double articulation, arranged on a tall and narrow facies articularis quadratica, is present in most palaeognaths, some Galliformes and Charadriiformes [36]. Remarkably, a third articulation occurs between the processus orbitalis of the quadrate and the processus articularis basipterygoideus, a feature not reported in any other fossil or extant birds. This may have significant functional implications for the entire palatal structure, suggesting a high degree of specialization, potentially related to its feeding ecology. Furthermore, the three well-developed crests on the pterygoid, which delimit broad surfaces, indicate associated powerful musculature, while the three anterior processes of the pterygoid suggest strong control of the articulation between this bone, the neurocranium, and the palatine. The pterygoid articulates with the rostrum parasphenoidale through a processus articularis basipterygoideus, which is dorsomedially elongated and very weakly developed in the rostrocaudal direction. In Galloanseres, on the contrary, the processus articularis basipterygoideus barely -or not at all- projects from the pes pterygoidei and is strongly developed anterioposteriorly. In both *Vegavis* and Galloanseres, this process is positioned close to the pterygopalatine articulation. The processus rostralis of the pterygoid articulates medially with the rostrum parasphenoidale and the dorsal surface of the palatine. The pterygopalatine articulation consists of a deep fossa on the pterygoid that receives the processus articularis pterygoideus of the palatine, which is situated laterally.

The processus basipterygoideus develops a unique shape, extending laterally from the rostrum parasphenoidale constituting a quadrangular shelf. Laterally expanded processus basipterygoideus are also observed in *Cerebavis* [29] in Procellariiformes and several Charadriiformes [69], and in *Muriwaimanu tuatahi* [70], among others. In contrast, the processus basipterygoideus of Galloanseres, Pelagornithidae, and Ichthyornithiformes, although poorly reconstructed in the latter [33,71], do not extend to the sides of the rostrum parasphenoidale; their articular surface faces ventrolaterally and the process consists of an oval surface [69,72–74]. In *V. geitononesos* (Figure 12), the articular surface is more elongated rostrocaudally than in *Muriwaimanu*, and furthermore, it does not form a "shelf". In Procellariiformes, the articular surface of the processus basipterygoideus is nearly circular.

The simultaneous presence of three well-developed ridges on the body of the pterygoid is unique to *Vegavis*. Although these ridges are present in other taxa [36], they never reach the degree of development observed in *Vegavis*. At its proximal end, three pointed processes of similar length surround a deep fossa; the process articulating with the basipterygoid is long and projects dorsally from the pes pterygoidei, whereas in Galloanseres it constitutes a flat surface elongated rostrocaudally. As in the latter, this process is located near the palato-pterygoid articulation. The rostral fossa articulates with the palatine, forming a "cup", as in Galloanseres and some Neoaves such as *Gavia* and *Puffinus* [36]. The palatine is surrounded laterally and medially by the two other processes of the pterygoid, the medial one being the longest (processus rostralis sensu Benito et al., 2022) [36]. A pointed processus rostralis is observed in *Dasornis*, *Nettapterornis*, and *Anatidae* [36].

At the caudal end, the articular surface for the quadrate is narrow but expands dorsoventrally in a fan shape, surrounding the quadrate. The articulation with the quadrate is double, like in Paleognathae, Galliformes, and some Charadriiformes, and unlike Anseriformes [12,30,75]), involving both the pterygoid condyle and the base of the orbital process

(orbitopterygoid facet sensu Kuo et al., 2023) [32]. This morphology is observed in most Gruiformes (Kuo et al., 2024: Supplementary Material) [76], as well as in *Larus* and *Gavia* among Neoaves, and in some Galliformes but not in Anseriformes [36]. Like in these birds and also in Ichthyornithiformes (Benito et al., 2022: extended data Figure 10c) [36], in *V. geitononesos* the articular fossa is on the pterygoid and the condylus on the quadrate.

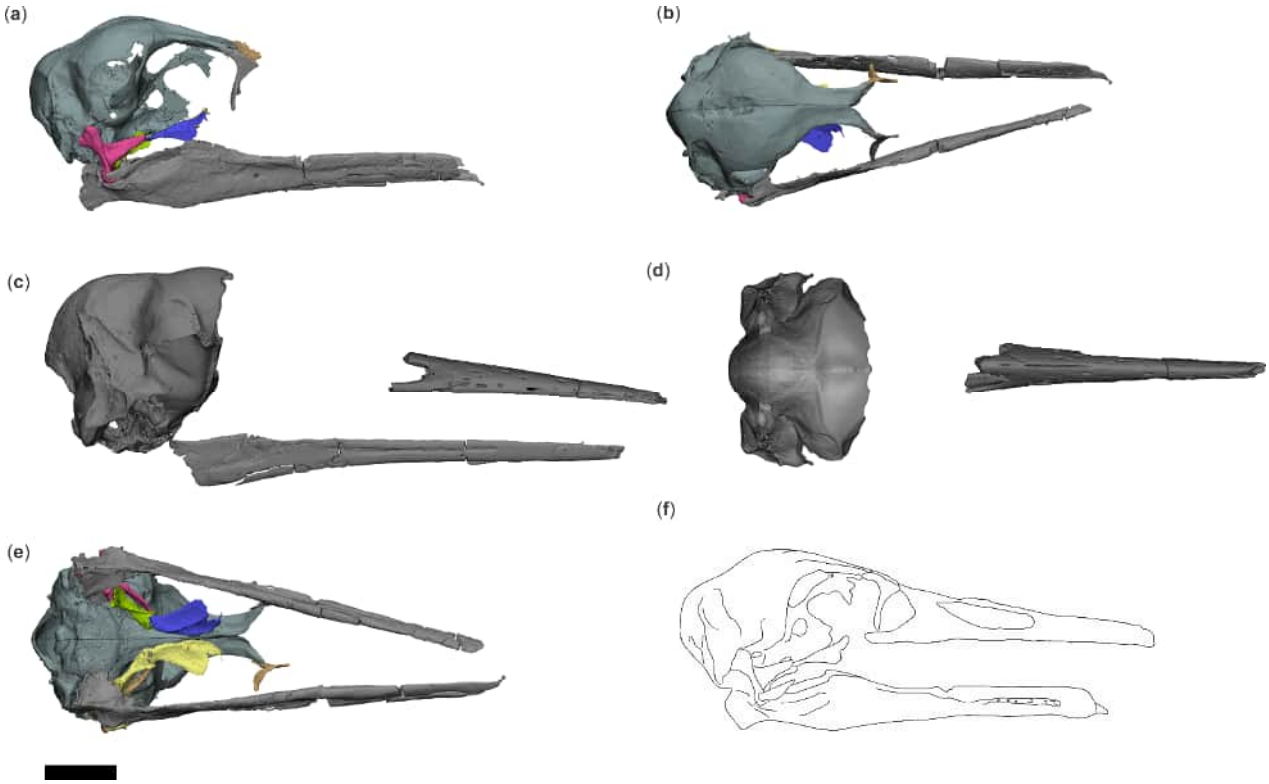

Figure 12. Virtual reconstructions of the skulls of V. *geitononesos* sp. nov. (MLP-PV 15-I-7-52) compared with *Pujatopouli soberana*. V. *geitononesos* in: (**a**) lateral, (**b**) dorsal, and (**e**) palatal view. *Pujatopouli soberana* in: (**c**) lateral, and (**d**) dorsal views. The drawing in (**f**) represents a reconstruction of the skull of *V. geitononesos* (the upper beak is based on *V. notopothousa* sp. nov. Scale bar = 10 mm.

The palatine articulates caudally and medially with the pterygoid, and medially with the rostrum parasphenoidale. Unlike in Ichthyornithiformes [33,71], the hemipterygoid is fused to the palatine, forming the processus articularis pterygoidei, a condition characteristic of Neognathae. The lateral margin of the palatine diverges laterorostrally, forming a concave edge; this morphology is uncommon among Neornithes and is shared with *Janavis* [36], *Aptenodytes* (juvenile specimen) [41], *Madrynornis* [37,38], and *Macronectes* [42]. Unlike the Galloanseres examined (*Alectoris*, *Alectura*, *Crax*, *Anas*, *Anser*, *Anseranas*, *Chauna*), the processus palatinus that articulates with the pterygoid is lateral, similar to the condition in juvenile *Spheniscus*, whereas it is medial in Galloanseres.

As detailed above, *Vegavis* exhibits a combination of palatal characters that can be traced across various Galloanseres and Neoaves. It also shows features that are unique among known Neornithes, such as a pterygoid with three rostral processes and three well-developed crests on the pterygoid body. This combination allows for a reevaluation of the galloanserine affinities of *Vegavis*.

The quadrate-mandibular articulation is bicondylar, a feature present in all extant Galloanseres and in some Neoaves (e.g., Columbiformes). The quadrate lacks the foramina typical of Galloanseres (specifically those described for Presbyornithidae by Elzanowski and Stidham (2010)) [30], and no foramina were observed. The processus orbitalis

is elongated and pointed, as in some Galloanseres and Aequolithornithes (Kuo et al., 2024: Supplementary Material) [76], and it bears a deep fovea quadratojugalis like that of most Aequornithes [76].

The retroarticular process of the mandible is short and bears a dorsal crest, forming part of a deep fossa caudalis, as in *Vegavis* and various Neoaves, including Charadriiformes and Aequornithes (Gaviiformes, Sphenisciformes, Procellariiformes, among others). In Galloanseres, the retroarticular process is caudally elongated, a condition also inferred in *Asteriornis*, the most basal known galloanserans [13,77].

V. geitononesos exhibits characters considered plesiomorphic for Neognathae, such as the presence of basipterygoid processes. However, it is important to note that the morphology of the basipterygoid processes in Ichthyornithiformes [36] consists of a flat, oval surface on the ventral side of the parasphenoid, as in Galloanseres, which may indicate that these taxa retain the plesiomorphic condition for Neornithes. Laterally expanded basipterygoid processes, like those of *V. geitononesos*, occur in extant Procellariiformes and stem Sphenisciformes [70], suggesting a derived condition, as in *Cerebavis*, whose uncertain systematic position hinders the establishment of character polarity. Shelf-like basipterygoid processes are unique to *V. geitononesos*. The crista ventralis present on the palatine has been cited as a diagnostic character of Neoaves [78]. This feature, combined with the shape of the pars lateralis—similar to that of some Sphenisciformes and Procellariiformes—and the distinctive morphology of the basipterygoid processes and the processus articularis basipterygoideus, which differ from those of known Galloanseres, allows us to hypothesize a closer relationship to Neoaves (possibly Aequornithes, as previously proposed for *Pujatopouli*) rather than to Galloanseres.

6.5. Paleoecological Implications

The marine environment represented in the López de Bertodano Formation was rich in foot-propelled diving birds [14,79]. The adaptations that enable this lifestyle and their relationship with the phylogenetic information they provide are strongly debated. Nevertheless, as in other extinct [80] and extant [81] marine birds, osteological and neuroanatomical differences among these birds suggest particular specializations within a single ecological guild, which, in our view, also correspond to taxonomic differences. This is evidenced by both estimated body masses and by osteological morphology and microstructure.

Body mass has a strong influence on diving and foraging ecology in many seabird species, such that greater body mass is positively correlated with longer and deeper dives in diving birds [82], a pattern further supported by a phylogenetically informed allometric analysis of diving performance [83]. This relationship is consistent with the physiological expectation that oxygen stores (in blood and muscle via myoglobin) scale approximately with body mass. In contrast, oxygen consumption scales more slowly, thereby extending dive capacity in larger birds [84]. In addition, larger body mass reduces thermal conductance, providing a thermoregulatory advantage for cold-water diving species and potentially allowing more sustained submersion or underwater foraging [85].

On this basis, body mass remains a key parameter for paleobiological and paleoecological reconstructions. Allometric relationships between skeletal measurements and body mass in extant birds allow the estimation of the mass of fossil taxa using different skeletal elements [20], enabling inferences about their likely ecology, locomotion, and niche.

The estimation of body masses clearly illustrates these differences (Table 1). Among the birds described to date from the Cretaceous of Antarctica, *Polarornis* is the heaviest (2820 g), followed by *Vegavis iaai* MLP-PV 93-I-3-1 (1189 or 1180 g, depending on whether the calculation is based on femoral circumference or the coracoid humeral facet), *Antarcticavis* (870 g), and finally *V. geitononesos* (696 g). For *Pujatopouli*, a mass of 2030 g was estimated,

although it was calculated based on the humerus, so its comparison with the other masses should be interpreted with caution. Occupying an intermediate position between *Polarornis* and *V. geitononesos* is the early Paleocene *Conflicto* (1642 g).

The osteosclerotic condition, characterized by the thickening and increase in density of bones, is a recurrent feature in a variety of secondarily aquatic vertebrates [86]. It has been documented in several groups of marine birds, particularly those that are strong or habitual divers [54]. In extant diving birds, increased bone mass has been interpreted as an adaptive response that enhances skeletal ballast, reducing buoyancy and facilitating subaqueous locomotion and prolonged submersion [86–88]. This condition is often accompanied by a reduction in skeletal pneumaticity, which further contributes to increased body density and improved diving efficiency [52]. Consequently, osteosclerosis in marine birds has important ecological implications, as it is associated with a more specialized diving lifestyle, access to deeper water columns, and a greater dependence on underwater foraging strategies compared to less densely ossified taxa.

In this context, the presence and variation in degree of pachyostotic or osteosclerotic conditions in certain Cretaceous Antarctic birds, such as *V. iaai* and *Polarornis gregorii*, indicate that these taxa developed skeletal modifications consistent with increased bone mass and density [1,89,90]. These features suggest that at least some of them were already highly adapted to a diving lifestyle.

Osteological variations evident in several elements of the skeleton among the Cretaceous Antarctic birds have been widely discussed in previous contributions [2,4,14,91]. In foot-propelled diving birds, the tarsometatarsus shows consistent ecomorphological associations with underwater locomotion [92]. Accordingly, the tarsometatarsus of *V. geitononesos* provides an opportunity to assess certain ecological parameters based on its comparatively lower degree of mediolateral shaft compression and hypotarsal morphology.

The less compressed tarsometatarsal shaft of *V. geitononesos*, relative to *V. iaai*, may indicate differences in hydrodynamic efficiency during submerged swimming [93], consistent with other features of the tarsometatarsus and femur.

In this context, the hypotarsus plays a critical role in the biomechanics of the foot, serving as an osteological pulley that guides the digital flexor tendons. This enables efficient force transmission during propulsion while minimizing lateral displacement or misalignment under loading [94]. In specialized Neornithes, the distal limb muscles and tendons underwent substantial reconfiguration, characterized by the expansion of the distal myotendinous apparatus and the development of accessory bony elements, constituting the different types of hypotarsus, which increased lever arms and improved control of digital flexion [94,95]. Consequently, hypotarsal configuration correlates with locomotor and ecological habits, ranging from simple or shallowly grooved hypotarsi, typical of terrestrial or cursorial forms, to more complex structures with multiple fully enclosed canals, characteristic of taxa with enhanced swimming capacities [19,93].

Many modern foot-propelled diving taxa exhibit a complex hypotarsus with well-defined canals, which likely ensures tendon alignment and protection under the hydrodynamic forces experienced during repeated swimming strokes [93]. In this context, the hypotarsus of *V. geitononesos*, with at least one fully enclosed canal, constitutes a specialized trait that along with other features like the curvature of the shaft and the condylar divergence of the femur, is consistent with a foot-propelled diving habit. The hypotarsal morphology of *V. geitononesos* implies elevated mechanical demands on the digital flexor tendons, a rigid tendon-guidance system, and a direct, forceful transmission of propulsive forces to the foot surface. These modifications are part of a broader hind limb functional complex in which the posterior placement of the limbs, the abovementioned femur modifica-

tions, and a consequent reorganization of musculature enhance the efficiency of propulsion during swimming [93].

V. geitononesos, as well as *V. iaai*, *V. notopothousa*, *Polarornis*, and *Pujatopouli*, participated in a radiation of foot-propelled diving birds in Antarctic marine ecosystems during the Maastrichtian [1,89]. This morphological diversification is also congruent with the general pattern of locomotor specialization observed in extant divers, which implies more sophisticated biomechanics of hindlimb-driven propulsion, closer to that of modern diving birds than to that of early, less specialized forms [96,97].

7. Conclusions

The anatomical osteological differences between the new specimen and the holotype and referred specimens of *Vegavis iaai* support the proposal of a second species within the genus. *V. geitononesos* sp. nov. is diagnosed by a unique combination of characters preserved in the mandible, pterygoids, femur, tarsometatarsus, synsacrum, and pelvis. In addition, morphological disparities between specimen AMNH FARB 30899 described by Torres et al. (2025) [6] and MACN-Pv 19.748 (the holotype of *V. iaai* MLP-PV 93-I-3-1 cannot be directly compared due to the absence of homologous elements), support the proposal of a third species within the genus. These differences, also noted by other authors [7,8], support the distinction of *V. notopothousa* sp. nov. as a distinct species of *Vegavis* based on its unique mandibular and basisphenoid morphology.

The quadrate–pterygoid–palatine–rostrum sphenoidale articulation is described here for the first time in a Cretaceous neornithine bird (Figure 12, Videos S1 and S2). Details of the most basal neognath-type palatal articulation are also presented, with comparisons to extant and fossil members of Galloanseres and Neoaves that highlight the synapomorphic and plesiomorphic states of the relevant palatal features.

A morphological affinity between *Vegavis* and Neoaves is also proposed, in contrast with earlier studies that placed it within Galloanserae [1–4,6,12,36]. However, most of the datasets used in the phylogenetic analyses of Cretaceous birds undersample the taxonomic diversity of Neoaves, which led to the placement of *Vegavis* within Galloanseres [14]. Furthermore, the lack of morphological data from the ancestral bauplan of Neoaves makes comparisons and character polarizations harder.

In line with our data, the Cretaceous marine environment of Marambio Island is interpreted as taxonomically diverse, hosting several species of marine diving birds of different sizes, each exhibiting distinct specializations within a shared ecological guild.

Supplementary Materials: The following supporting information can be downloaded at https://www.mdpi.com/article/10.3390/d18020082/s1: Figure S1: Block containing the skeleton; Video S1: Virtual reconstruction *Vegavis geitononesos* sp. nov.; Video S2: Virtual reconstruction *Vegavis geitononesos* sp. nov.

Author Contributions: Conceptualization, F.I. and C.A.H.; methodology, F.I., C.A.H. and A.P.-C.; software, F.I. and N.V.; validation, F.I., C.A.H. and A.P.-C.; formal analysis, F.I.; investigation, F.I., C.A.H. and A.P.-C.; resources, F.I., C.A.H. and A.P.-C.; data curation, F.I.; writing—original draft preparation, F.I., C.A.H. and A.P.-C.; writing—review and editing, F.I., C.A.H., A.P.-C., P.B. and N.V.; supervision, F.I., C.A.H. and A.P.-C.; project administration, F.I., C.A.H. and A.P.-C.; funding acquisition, F.I., C.A.H. and A.P.-C. All authors have read and agreed to the published version of the manuscript.

Funding: This research was funded by UNLP 11/N1044, 11/1063 and CONICET PIP 0096.

Data Availability Statement: The data that support the findings of this study are housed in Morphobank (Project 6179: New Vegavis. Diversity.) The password for reviewers is "marambio".

Acknowledgments: We thank Martín de los Reyes (MLP) for the access to the material; the Vertebrate Paleontology Group of the División Paleontología Vertebrados (MLP-UNLP) and the IAA (DNA) for their logistical support and fieldwork assistance; Leonel Acosta (MLP) for the exquisite specimen preparation; Federico Agnolín for access to the Vegavis specimen housed at the MACN; and Julio "Pelu" Muiño from the Hospital Interzonal General de Agudos "General San Martín" in La Plata city (Buenos Aires Province, Argentina) for the scanning facilities. We also acknowledge the support of the Centro Atómico Constituyentes, Comisión Nacional de Energía Atómica. We thanks to the four reviewers and the editor.

Conflicts of Interest: The authors declare no conflicts of interest.

References

1. Clarke, J.A.; Tambussi, C.P.; Noriega, J.I.; Erickson, G.M.; Ketcham, R.A. Definitive fossil evidence for the extant avian radiation in the Cretaceous. *Nature* **2005**, *433*, 305–308. [CrossRef] [PubMed]
2. Clarke, J.A.; Chatterjee, S.; Li, Z.; Riede, T.; Agnolin, F.; Goller, F.; Isasi, M.P.; Martinioni, D.R.; Mussel, F.J.; Novas, F.E. Fossil evidence of the avian vocal organ from the Mesozoic. *Nature* **2016**, *538*, 502–505. [CrossRef]
3. Noriega, J.I.; Tambussi, C.P. A Late Cretaceous Presbyornithidae (Aves: Anseriformes) from Vega Island, Antarctic Peninsula: Paleobiogeographic implications. *Ameghiniana* **1995**, *32*, 57–61.
4. Acosta Hospitaleche, C.; Worthy, T.H. New data on the *Vegavis iaai* holotype from the Maastrichtian of Antarctica. *Cretac. Res.* **2021**, *124*, 104818. [CrossRef]
5. Alvarez-Herrera, G.P.; Rozadilla, S.; Agnolín, F.L.; Novas, F.E. Jaw anatomy of *Vegavis iaai* (Clarke et al., 2005) from the Late Cretaceous Antarctica, and its phylogenetic implications. *Geobios* **2024**, *83*, 11–20. [CrossRef]
6. Torres, C.R.; Clarke, J.A.; Groenke, J.R.; Lamanna, M.C.; MacPhee, R.D.; Musser, G.M.; Sertich, J.J.W.; O'Connor, P.M. Cretaceous Antarctic bird skull elucidates early avian ecological diversity. *Nature* **2025**, *638*, 146–151. [CrossRef] [PubMed]
7. Field, D.J. Paleontology: Ducks all the way down? *Curr. Biol.* **2025**, *35*, R409–R412. [CrossRef]
8. Crane, A.H.; Benito, J.; Chen, A.; Ksepka, D.T.; Field, D.J. Mandibular morphology clarifies phylogenetic relationships near the origin of crown birds. *BMC Ecol. Evo.* **2025**, *26*, 11. [CrossRef]
9. De Souza, G.A.; Bulak, B.A.; Soares, M.B.; Sayão, J.M.; Weinschütz, L.C.; Batezelli, A.; Kellner, A.W. The Cretaceous Neornithine record and new Vegaviidae specimens from the López de Bertodano Formation (Upper Maastrichtian) of Vega Island, Antarctic Peninsula. *An. Acad. Bras. Ciênc.* **2023**, *95*, e20230802. [CrossRef]
10. Case, J.; Reguero, M.; Martin, J.; Cordes-Person, A. A cursorial bird from the Maastrichtian of Antarctica. *J. Verteb. Paleont.* **2006**, *26*, 48A.
11. West, A.R.; Torres, C.R.; Case, J.A.; Clarke, J.A.; O'Connor, P.M.; Lamanna, M.C. An avian femur from the Late Cretaceous of Vega Island, Antarctic Peninsula: Removing the record of cursorial landbirds from the Mesozoic of Antarctica. *PeerJ* **2019**, *7*, e7231. [CrossRef]
12. Worthy, T.H.; Degrange, F.J.; Handley, W.D.; Lee, M.S.Y. The evolution of giant flightless birds and novel phylogenetic relationships for extinct fowl (Aves, Galloanseres). *R. Soc. Open Sci.* **2017**, *4*, 170975. [CrossRef]
13. Field, D.J.; Benito, J.; Chen, A.; Jagt, J.W.M.; Ksepka, D.T. Late Cretaceous neornithine from Europe illuminates the origins of crown birds. *Nature* **2020**, *579*, 397–401. [CrossRef]
14. Irazoqui, F.; Acosta Hospitaleche, C.; Gelfo, J.N.; Carabajal, A.P.; Bona, P.; Burlaille, L.A. Diving in the Maastrichtian of Marambio (Seymour) Island: A new member of the Neoaves in the Cretaceous Antarctic avifauna. *Cretac. Res.* **2025**, *165*, 106259. [CrossRef]
15. Agnolín, F.L.; Egli, F.B.; Chatterjee, S.; Marsà, J.A.G.; Novas, F.E. Vegaviidae, a new clade of southern diving birds that survived okthe K/T boundary. *Sci. Nat.* **2017**, *104*, 87. [CrossRef]
16. Mayr, G.; De Pietri, V.L.; Scofield, R.P.; Worthy, T.H. On the taxonomic composition and phylogenetic affinities of the recently proposed clade Vegaviidae Agnolín et al., 2017—neornithine birds from the Upper Cretaceous of the Southern Hemisphere. *Cretac. Res.* **2018**, *86*, 178–185. [CrossRef]
17. McLachlan, S.M.S.; Kaiser, G.W.; Longrich, N.R. *Maaqwi cascadensis*: A large, marine diving bird (Avialae: Ornithurae) from the Upper Cretaceous of British Columbia, Canada. *PLoS ONE* **2017**, *12*, e0189473. [CrossRef] [PubMed]
18. Baumel, J.J.; Witmer, L.M. Osteologia. In *Handbook of Avian Anatomy: Nomina Anatomica Avium*, 2nd ed.; Baumel, J.J., Ed.; Publications of the Nuttall Ornithological Club: Cambridge, MA, USA, 1993; pp. 45–132.
19. Mayr, G. Variations in the hypotarsus morphology of birds and their evolutionary significance. *Acta Zool.* **2016**, *97*, 196–210. [CrossRef]
20. Field, D.J.; Lynner, C.; Brown, C.; Darroch, S.A. Skeletal correlates for body mass estimation in modern and fossil flying birds. *PLoS ONE* **2013**, *8*, e82000. [CrossRef]

21. Rinaldi, C.; Massabie, A.; Morelli, J.; Rosenman, L.; Del Valle, R. *Geología de la Isla Vicecomodoro Marambio, Antártida*; Instituto Antártico Argentino: Buenos Aires, Argentina, 1978; Volume 217, pp. 1–37.
22. Macellari, C. Stratigraphy, sedimentology, and paleoecology of Upper Cretaceous/Paleocene shelf-deltaic sediments of Seymour Island. In *Geology and Paleontology of Seymour Island, Antarctic Peninsula*; Feldmann, R.M., Woodburne, M.O., Eds.; Geological Society of America: Boulder, CO, USA, 1988; Volume 169, pp. 25–53.
23. Marenssi, S.; Santillana, S.; Rinaldi, C. Stratigraphy of La Meseta Formation (Eocene), Marambio Island, Antarctica. *Rev. Asoc. Paleontol. Argent. Publ. Espec.* **1998**, *5*, 137–146.
24. Montes, M.; Nozal, F.; Olivero, E.; Gallastegui, G.; Santillana, S.; Maestro, A.; López-Martínez, J.; González, L.; Martín-Serrano, A. Geología y geomorfología de Isla Marambio (Seymour). In *Geología y Geomorfología de Isla Marambio (Seymour)*; Montes, M., Nozal, F., Eds.; Instituto Geológico y Minero de España: Madrid, Spain; Instituto Antártico Argentino: Buenos Aires, Argentina, 2019.
25. Olivero, E.; Ponce, J.; Martinioni, D. Sedimentology and architecture of sharp-based tidal sandstones in the Upper Marambio Group, Maastrichtian of Antarctica. *Sediment. Geol.* **2008**, *210*, 11–26. [CrossRef]
26. Crame, J.; Francis, J.; Cantrill, D.; Pirrie, D. Maastrichtian stratigraphy of Antarctica. *Cretac. Res.* **2004**, *25*, 411–423. [CrossRef]
27. Olivero, E.; Medina, F. Patterns of Late Cretaceous ammonite biogeography in southern high latitudes: The Family Kossmaticeratidae in Antarctica. *Cretac. Res.* **2000**, *21*, 269–279. [CrossRef]
28. International Union of Geological Sciences. *The First 100 IUGS Geological Heritage Sites: Cretaceous–Paleogene Transition at Seymour (Marambio) Island (Site 021)*; IUGS: Paris, France, 2022.
29. Walsh, S.A.; Milner, A.C.; Bourdon, E. A reappraisal of *Cerebavis cenomanica* (Aves, ornithurae), from Melovatka, Russia. *J. Anat.* **2016**, *229*, 215–227. [CrossRef]
30. Tambussi, C.P.; Degrange, F.J.; De Mendoza, R.S.; Sferco, E.; Santillana, S. A stem anseriform from the early Palaeocene of Antarctica provides new key evidence in the early evolution of waterfowl. *Zool. J. Linn. Soc.* **2019**, *186*, 673–700. [CrossRef]
31. Elzanowski, A.; Stidham, T.A. Morphology of the quadrate in the Eocene anseriform Presbyornis and extant galloanserine birds. *J. Morphol.* **2010**, *271*, 305–323. [CrossRef]
32. Kuo, P.C.; Benson, R.B.; Field, D.J. The influence of fossils in macroevolutionary analyses of 3D geometric morphometric data: A case study of galloanseran quadrates. *J. Morphol.* **2023**, *284*, e21594. [CrossRef] [PubMed]
33. Field, D.J.; Hanson, M.; Burnham, D.; Wilson, L.E.; Super, K.; Ehret, D.; Ebersole, J.A.; Bhullar, B.A.S. Complete Ichthyornis skull illuminates mosaic assembly of the avian head. *Nature* **2018**, *557*, 96–100. [CrossRef]
34. Wang, M.; Li, D.; O'Connor, J.K.; Zhou, Z.; You, H. Second species of enantiornithine bird from the Lower Cretaceous Changma Basin, northwestern China with implications for the taxonomic diversity of the Changma avifauna. *Cret. Res.* **2015**, *55*, 56–65. [CrossRef]
35. Wang, M.; Hu, H. A comparative morphological study of the jugal and quadratojugal in early birds and their dinosaurian relatives. *Anatom. Rec.* **2017**, *300*, 62–75. [CrossRef] [PubMed]
36. Benito, J.; Kuo, P.-C.; Widrig, K.E.; Jagt, J.W.M.; Field, D.J. Cretaceous ornithurine supports a neognathous crown bird ancestor. *Nature* **2022**, *612*, 100–105. [CrossRef]
37. Acosta Hospitaleche, C.; Tambussi, C.; Donato, M.; Cozzuol, M. A new Miocene penguin from Patagonia and its phylogenetic relationships. *Acta Palaeontol. Pol.* **2007**, *52*, 299–314.
38. Degrange, F.J.; Ksepka, D.T.; Tambussi, C.P. Redescription of the oldest crown clade penguin: Cranial osteology, jaw myology, neuroanatomy, and phylogenetic affinities of *Madrynornis mirandus*. *J. Vertebr. Paleontol.* **2018**, *38*, e1445636. [CrossRef]
39. Starck, J.M.; Chinsamy, A. Bone histology of birds. In *Bone Histology of Fossil Tetrapods*; Chinsamy-Turan, A., Ed.; University of California Press: Berkeley, CA, USA, 2002; pp. 149–179.
40. Tumarkin-Deratzian, A.R.; Vann, D.R.; Dodson, P. Bone surface texture as an ontogenetic indicator in long bones of the Canada goose Branta canadensis (Anseriformes: Anatidae). *Zool. J. Linn. Soc.* **2006**, *148*, 133–168. [CrossRef]
41. Sosa, M.A.; Acosta Hospitaleche, C. Ontogenetic variations of the head of *Aptenodytes forsteri* (Aves, Sphenisciformes): Muscular and skull morphology. *Polar Biol.* **2018**, *41*, 225–235. [CrossRef]
42. Piro, A.; Acosta Hospitaleche, C. Skull morphology and ontogenetic variation of the Southern Giant Petrel *Macronectes giganteus* (Aves: Procellariiformes). *Polar Biol.* **2019**, *42*, 27–45. [CrossRef]
43. Bailleul, A.M.; Scannella, J.; Horner, J.; Evans, D. Fusion patterns in the skulls of modern archosaurs reveal that sutures are ambiguous maturity indicators for the Dinosauria. *PLoS ONE* **2016**, *11*, e0147687. [CrossRef]
44. Schmid, E.; Tütken, T.; Wings, O. *Bone Histology of Birds*; Wiley-Blackwell: Chichester, UK, 2013.
45. Maxwell, E.E.; Harrison, L.B.; Larsson, H.C. Assessing the phylogenetic utility of sequence heterochrony: Evolution of avian ossification sequences as a case study. *Zoology* **2010**, *113*, 57–66. [CrossRef] [PubMed]
46. Plateau, O.; Green, T.L.; Gignac, P.M.; Foth, C. Comparative digital reconstruction of *Pica pica* and *Struthio camelus* and their cranial suture ontogenies. *Anat. Rec.* **2024**, *307*, 5–48.
47. Watanabe, J. Ontogeny of macroscopic morphology of limb bones in modern aquatic birds and their implications for ontogenetic ageing. *Contrib. MACN* **2017**, *7*, 183–220.

48. Watanabe, J. Ontogeny of surface texture of limb bones in modern aquatic birds and applicability of textural ageing. *Anat. Rec.* **2018**, *301*, 1026–1045.
49. Maxwell, E.E. Ossification sequence of the avian order Anseriformes, with comparison to other precocial birds. *J. Morphol.* **2008**, *269*, 1095–1113. [CrossRef] [PubMed]
50. Acosta Hospitaleche, C.; Picasso, M.J. Textural ageing in *Pygoscelis antarctica* (Aves, Sphenisciformes): A new comparative scale for penguin bones. *Vertebr. Zool.* **2020**, *70*, 125–139.
51. Carrier, D.; Leon, L.R. Skeletal growth and function in the California gull (*Larus californicus*). *J. Zool.* **1990**, *222*, 375–389.
52. Habib, M.B.; Ruff, C.B. The effects of locomotion on limb bone structure in birds. *Zool. J. Linn. Soc.* **2008**, *153*, 601–624.
53. Ksepka, D.T.; Werning, S.; Sclafani, M.; Boles, Z.M. Bone histology in extant and fossil penguins (Aves: Sphenisciformes). *J. Anat.* **2015**, *227*, 611–630.
54. De Mendoza, R.S.; Tambussi, C.P. Osteosclerosis in the extinct *Cayaoa bruneti* (Aves, Anseriformes): Insights on behavior and flightlessness. *Ameghiniana* **2015**, *52*, 305–313. [CrossRef]
55. Kriloff, A.; Germain, D.; Canoville, A.; Vincent, P.; Sache, M.; Laurin, M. Patterns of bone density in diving birds. *J. Morphol.* **2008**, *269*, 532–541.
56. Griffin, C.T.; Stocker, M.R.; Colleary, C.; Stefanic, C.M.; Lessner, E.J.; Riegler, M.; Formoso, K.K.; Koeller, K.; Nesbitt, S.J. Assessing ontogenetic maturity in extinct saurian reptiles. *Biol. Rev.* **2021**, *96*, 470–525.
57. Watanabe, J.; Matsuoka, H. Ontogenetic change of morphology and surface texture of long bones in the Gray Heron (*Ardea cinerea*, Ardeidae). In Proceedings of the 8th International Meeting of the Society of Avian Paleontology and Evolution, Vienna, Austria, 12–16 June 2012; pp. 279–306.
58. Székely, T.; Lislevand, T.; Figuerola, J. Sexual size dimorphism in birds. In *Sex, Size and Gender Roles: Evolutionary Studies of Sexual Size Dimorphism*; Fairbairn, D.J., Blanckenhorn, W.U., Székely, T., Eds.; Oxford University Press: Oxford, UK, 2007; pp. 27–37.
59. Livezey, B.C.; Humphrey, P.S. Sexual dimorphism in continental steamer-ducks. *Condor* **1984**, *86*, 368–377. [CrossRef]
60. Handley, W.D.; Chinsamy, A.; Yates, A.M.; Worthy, T.H. Sexual dimorphism in the late Miocene mihirung Dromornis stirtoni (Aves: Dromornithidae) from the Alcoota Local Fauna of central Australia. *J. Verteb. Paleont.* **2016**, *36*, e1180298. [CrossRef]
61. Livezey, B.C. Morphometric patterns in recent and fossil penguins (Aves, Sphenisciformes). *J. Zool.* **1989**, *219*, 269–307. [CrossRef]
62. Kerry, K.R.; Agnew, D.J.; Clarke, J.R.; Else, G.D. Use of morphometric parameters for the determination of sex of Adelie Penguins. *Wildl. Res.* **1992**, *19*, 657–664. [CrossRef]
63. Serrano-Meneses, M.A.; Székely, T. Sexual size dimorphism in seabirds: Sexual selection, fecundity selection and differential niche-utilisation. *Oikos* **2006**, *113*, 385–394. [CrossRef]
64. Einoder, L.D.; Page, B.; Goldsworthy, S.D. Sexual size dimorphism and assortative mating in the Short-tailed Shearwater *Puffinus tenuirostris*. *Mar. Ornithol.* **2008**, *36*, 167–173. [CrossRef]
65. Pazvant, G.; İnce, N.G.; Özkan, E.; Gündemir, O.; Avanus, K.; Szara, T. Sex determination based on morphometric measurements in yellow-legged gulls (*Larus michahellis*) around Istanbul. *BMC Zool.* **2022**, *7*, 35. [CrossRef] [PubMed]
66. Aina, O.O.; Ekeolu, O.K. Sexual Dimorphism of the Pelvic Bone and Limbs of *Francolinus bicalcaratus*. *Savannah Vet. J.* **2021**, *4*, 49–55.
67. Chatterjee, S. The morphology and systematics of *Polarornis*, a Cretaceous loon (Aves: Gaviidae) from Antarctica. In *Proceedings of the 5th Symposium of the Society of Avian Paleontology and Evolution, Beijing, China, 1–4 June 2000*; Zhou, Z., Zhang, F., Eds.; Science Press: Beijing, China, 2002; pp. 125–155.
68. Brownstein, C.D. A juvenile bird with possible crown-group affinities from a dinosaur-rich Cretaceous ecosystem in North America. *BMC Ecol. Evol.* **2024**, *24*, 20.
69. Elzanowski, A. On the role of basipterygoid processes in some birds. *Verh. Anat. Ges.* **1977**, *71*, 1303–1307.
70. Mayr, G.; De Pietri, V.L.; Proffitt, J.; Blokland, J.C.; Clarke, J.A.; Love, L.; Mannering, A.A.; Scofield, R.P. Multiple exceptionally preserved fossils from the Paleocene Waipara Greensand inform the diversity of the oldest stem group Sphenisciformes and the formation of their diving adaptations. *Zool. J. Linn. Soc.* **2025**, *204*, zlaf080. [CrossRef]
71. Wilken, A.T.; Sellers, K.C.; Davis, J.L.; Witmer, L.M.; Holliday, C.M. Reply to Benito et al.: Problems in the Cretaceous evolution of the avian palatobasal joint. *Proc. Natl. Acad. Sci. USA* **2026**, *123*, e2520865123. [CrossRef]
72. Bock, W.J. Kinetics of the avian skull. *J. Morphol.* **1964**, *114*, 1–42. [CrossRef]
73. Acosta Hospitaleche, C.I.; Piro, A.; Sosa, M.A. The mandibulosphenoidal joint in penguins, albatrosses, and petrels: Comparative anatomy and functional implications. *Vert. Zool.* **2020**, *12*, 118.
74. Houde, P.; Dickson, M.; Camarena, D. Basal anseriformes from the early Paleogene of North America and Europe. *Diversity* **2023**, *15*, 233. [CrossRef]
75. Elzanowski, A.; Stidham, T.A. A galloanserine quadrate from the Late Cretaceous Lance Formation of Wyoming. *Auk* **2011**, *128*, 138–145. [CrossRef]
76. Kuo, P.-C.; Navalón, G.; Benson, R.B.J.; Field, D.J. Macroevolutionary drivers of morphological disparity in the avian quadrate. *Proc. R. Soc. B* **2024**, *291*, 20232250. [CrossRef]

77. Crane, A.; Benito, J.; Chen, A.; Musser, G.; Torres, C.R.; Clarke, J.A.; Lamanna, M.C.; O'Connor, P.M.; Ksepka, D.T.; Field, D.J. Taphonomic damage obfuscates interpretation of the retroarticular region of the *Asteriornis* mandible. *Geobios* **2025**, *90*, 31–43. [CrossRef]
78. Mayr, G. Cenozoic mystery birds—On the phylogenetic affinities of bony-toothed birds (Pelagornithidae). *Zool. Scr.* **2011**, *40*, 448–467. [CrossRef]
79. Acosta Hospitaleche, C.; Irazoqui, F.; Bona, P.; Paulina-Carabajal, A. Review of the Cretaceous avian diversity of Antarctica: A changing scenario for the evolution of early Neornithine birds. *Adv. Polar Sci.* **2024**, *35*, 1–13. [CrossRef]
80. Bell, A.; Chiappe, L.M. The Hesperornithiformes: A review of the diversity, distribution, and ecology of the earliest diving birds. *Diversity* **2022**, *14*, 267. [CrossRef]
81. Petalas, C.; Lazarus, T.; Layoie, R.A.; Elliott, K.H.; Guigueno, M.F. Foraging niche partitioning in sympatric seabird populations. *Sci. Res.* **2021**, *11*, 2493. [CrossRef] [PubMed]
82. Watanuki, Y.; Burger, A.E. Body mass and dive duration in alcids and penguins. *Can. J. Zool.* **1999**, *77*, 1838–1842. [CrossRef]
83. Halsey, L.G.; Blackburn, T.M.; Butler, P.J. A comparative analysis of the diving behaviour of birds and mammals. *Funct. Ecol.* **2006**, *20*, 889–899. [CrossRef]
84. Kooyman, G.L.; Ponganis, P.J. The physiological basis of diving to depth: Birds and mammals. *Annu. Rev. Physiol.* **1998**, *60*, 19–32. [CrossRef]
85. de Vries, J.; van Eerden, M.R. Thermal conductance in aquatic birds in relation to the degree of water contact, body mass, and body fat: Energetic implications of living in a strong cooling environment. *Physiol. Zool.* **1995**, *68*, 1143–1163. [CrossRef]
86. Houssaye, A. "Pachyostosis" in aquatic amniotes: A review. *Integr. Zool.* **2009**, *4*, 325–340. [CrossRef]
87. Taylor, M.A. Functional significance of bone ballastin in the evolution of buoyancy control strategies by aquatic tetrapods. *Hist. Biol.* **2000**, *14*, 15–31. [CrossRef]
88. Dumont, M.; Laurin, M.; Jacques, F.; Pellé, E. Inner architecture of vertebral bone in terrestrial and aquatic amniotes and its relation to density. *J. Morphol.* **2013**, *274*, 1089–1100. [CrossRef]
89. García Marsà, J.A.; Agnolín, F.; Novas, F.E. Bone microstructure of *Vegavis iaai* (Aves, Anseriformes) from the Upper Cretaceous of Vega Island, Antarctic Peninsula. *Hist. Biol.* **2019**, *31*, 163–167. [CrossRef]
90. Fabbri, M.; Navalón, G.; Benson, R.B.; Pol, D.; O'Connor, J.; Bhullar, B.A.S.; Erickson, G.M.; Norell, M.A.; Orkney, A.; Lamanna, M.C.; et al. Subaqueous foraging among carnivorous dinosaurs. *Nature* **2022**, *603*, 852–857. [CrossRef]
91. Cordes-Person, A.; Acosta Hospitaleche, C.; Case, J.; Martin, J. An enigmatic bird from the lower Maastrichtian of Vega Island, Antarctica. *Cretac. Res.* **2020**, *108*, 104314. [CrossRef]
92. De Mendoza, R.S.; Gómez, R.O. Ecomorphology of the tarsometatarsus of waterfowl (Anseriformes) based on geometric morphometrics and its application to fossils. *Anat. Rec.* **2022**, *305*, 3243–3253. [CrossRef]
93. Clifton, G.T.; Carrano, M.T.; Hutchinson, J.R. Evolution of pelvic limb muscle moment arms in birds and their relationship to locomotor behaviour. *Proc. R. Soc. B* **2018**, *285*, 20171766.
94. Hutchinson, J.R. The evolution of hindlimb tendons and muscles on the line to crown-group birds. *Comp. Biochem. Physiol. A* **2002**, *133*, 1051–1086.
95. Hutchinson, J.R.; Allen, V. The evolutionary continuum of limb function from early theropods to birds. *Naturwissenschaften* **2009**, *96*, 423–448.
96. Zeffer, A.; Johansson, L.C.; Marmebro, Å. Functional correlation between habitat use and leg morphology in birds (Aves). *Biol. J. Linn. Soc.* **2003**, *79*, 461–484. [CrossRef]
97. Doube, M.; Yen, S.C.; Kłosowski, M.M.; Farke, A.A.; Hutchinson, J.R.; Shefelbine, S.J. Whole-bone scaling of the avian pelvic limb. *J. Anat.* **2012**, *221*, 21–29. [CrossRef] [PubMed]